Voltage-dependent P-Q Reserve Capacity Evaluation for TSO-DSO Interface Considering Uncertainties of DGs and FLs

Yeyan Xu, Liangzhong Yao, *Fellow*, *IEEE*, Tianjiao Pu, *Senior Member*, *IEEE*, *Fellow*, *CSEE*, Siyang Liao, *Member*, *IEEE*, *Member*, *CSEE*, Fan Cheng, Ye Li, and Xinying Wang, *Senior Member*, *IEEE*, *Senior Member*, *CSEE*

***Abstract*—Increasing distributed generators (DGs) and flexible loads (FLs) enable distribution systems to provide both active and reactive power reserves (P-Q reserves) in supporting the frequency and voltage regulations of transmission systems. However, such requirements at the interface between the transmission system operator (TSO) and distribution system operator (DSO) affect the distribution system operation security, considering the uncertainties of DGs and FLs. To exploit the reserve potential of distribution systems, this paper investigates the voltage-dependent P-Q reserve capacity (V-PQRC) of such types of distribution systems. V-PQRC reflects the feasible space of P-Q reserves that the DSO can provide to the TSO taking the voltage deviation limit at TSO-DSO interface into consideration, while ensuring the distribution system operation security under uncertainties of DGs and FLs. An evaluation method for V-PQRC at the TSO-DSO interface is proposed. To improve the robust performance of the evaluation method, the DG uncertainty is captured by a generalized ambiguity set and the FL uncertainty is addressed by designing a constrained sliding mode controller (CSMC). Three objectives are considered in the evaluation, i.e., P reserve capacity, Q reserve capacity, and the voltage deviation limit at the TSO-DSO interface. Then, a multi-objective optimization model integrating the generalized robust chance-constrained optimization and CSMC (GRCC-CSMC) is established for V-PQRC evaluation to obtain the Pareto optimal reserve schemes. Finally, a non-approximated selecting (NAS) method is proposed to build up a simplified V-PQRC linear model, which can be convenient to apply in the transmission-distribution system coordination. Simulation results reveal that the V-PQRC evaluation method can achieve a good performance of accuracy and robustness against uncertainties.**

***Index Terms*—Generalized robust chance-constrained optimization, reserve capacity evaluation, sliding mode control, transmission-distribution system coordination, voltage-dependent P-Q reserve capacity.**

Manuscript received January 12, 2022; revised April 14, 2022; accepted May 27, 2022. Date of online publication August 18, 2022; date of current version July 19, 2023. This work was supported by the National Key R&D Program of China (2020YFB0905900); Science and Technology Project of SGCC (State Grid Corporation of China): The key Technologies for Electric Internet of Things (SGTJDK00DWJS2100042).

Y. Y. Xu, L. Z. Yao (corresponding author, email: yaoliangzhong@whu.edu.cn), and S. Y. Liao are with the School of Electrical Engineering and Automation, Wuhan University, Wuhan 430072, China.

F. Cheng was with China Electric Power Research Institute, Beijing 100085, China.

T. J. Pu, Y. Li, and X. Y. Wang are with China Electric Power Research Institute, Beijing 100192, China.

DOI: 10.17775/CSEEJPES.2022.00360

I. Introduction

THE increasing penetration of intermittent renewable energy resources has brought serious challenges to frequency and voltage stability of transmission systems. Since synchronous generators are gradually replaced by the renewable energy resources, the transmission system lacks sufficient active power reserves (P reserves) and reactive power reserves (Q reserves) to support frequency and voltage regulations. Therefore, it is crucial for the transmission system operator (TSO) to find alternative reserve resources.

Distribution systems integrated with distributed generators (DGs) and flexible loads (FLs) have a great potential to provide both P and Q reserves in support of the frequency and voltage regulations in transmission systems [1], [2]. In this paper, DGs refer to the distributed renewable energy resources, such as distributed wind and photovoltaic power generations. The distribution system operator (DSO) can control the internal DGs and FLs to change the active and reactive power flows at the TSO-DSO interface, to equivalently provide localized P reserves and Q reserves for the transmission system. It is believed to be more economical than installing additional energy storage or var devices in transmission systems if DGs and FLs are controlled properly [3].

In terms of the transmission-distribution (T-D) system coordination, the T-D system coordinated dispatch methods in [4]–[6] optimize the output power of conventional generators and DGs in the distribution system, to compensate the P reserve shortage of the transmission system. In [7], FLs are aggregated to provide primary frequency regulation reserves for the transmission system. In [8], the Q reserve capacity of the Swiss distribution system is evaluated to provide voltage support for the transmission system. In [9], the optimal reactive power dispatch is utilized to maximize the reactive power support of DGs connected in a Germany 110 kV grid for the transmission grid. In [10], the DG reactive output power is coordinated with the load tap changers inside distribution systems to maintain the voltage security of transmission and distribution systems. In [11], a linear Q reserve capacity analysis model is proposed to evaluate the reactive power support potential of radial distribution systems.

From existing publications, P and Q reserves are separately evaluated and optimized, which may confront the risk of

resource conflicts. DGs and FLs are the shared resources for both P and Q reserves. The separate P (or Q) reserve evaluation result may not be executable due to the limited reserve ability of DGs and FLs. To avoid such problems, it is necessary to coordinately evaluate the P-Q reserve capacity (PQRC).

In this regard, [12] defines the upper and lower limits of the Q reserve as a function of the active exchange power at the TSO-DSO interface. In [13], the Monte Carlo Simulation is used to calculate the feasible range of the active and reactive exchange power at the TSO-DSO interface. In [14], [15], the P-Q exchange power of the distribution systems at the TSO-DSO interface is regarded as a 2-dimensional (2-D) polygon area on the P-Q plane. The concept of the linear weighted sum method is employed to solve the two-objective optimization problem. The above publications all assume that the voltage at the TSO-DSO interface is fixed during the whole dispatch interval. However, in practice, the voltage at the TSO-DSO interface will change when the DSO provides the P-Q power support to TSO or the TSO actions for frequency or voltage regulations, which will in turn affect the voltage security inside the distribution system. [16] involves the impact of voltage deviation at the TSO-DSO interface in evaluating the reactive power potential of distribution systems, to ensure the voltage security inside distribution systems. However, only the Q reserve is investigated in [16]. At present, the PQRC evaluation considering the voltage deviation at the TSO-DSO interface is relatively rare.

The uncertainties of DGs and FLs are another challenging issue for PQRC evaluation. The two-stage robust optimization method is utilized in [16] to ensure the reliability of evaluation results for any possible instance of the uncertainty set. To reduce the computation burden, the one-stage distributionally robust chance-constrained optimization method is utilized in [17], [18] to ensure the chance constraint to be satisfied for any distribution in the ambiguity set, by limiting its infimum probability. Diverse ambiguity sets have been designed based on moment or metric information, to cover the possible distributions of uncertainties. A moment-based ambiguity set with the known mean and covariance matrix is designed in [19] to capture the distributions of DG and load uncertainties. A Wasserstein metric-based ambiguity set is modeled in [20] according to the empirical distribution. A piecewise-linear-function-based ambiguity set is established in [21] to capture the uncertainties of sources and loads. In [22], a generalized ambiguity set is designed to enhance the robustness with inadequate historical data. The one-stage generalized robust chance-constrained optimization (GRCC) method is proposed in [23] to ensure the chance constraints are reliable for any possible uncertainty captured by the generalized ambiguity set.

Different from above publications that characterize the uncertainties of different resources by one ambiguity set, [24] separately handles risks of market-related uncertainties and solar-related uncertainties. [25] decomposes the high-dimensional robust optimization problem into a few simple sub-problems by classifying the uncertainty variables. The results indicate that separately treating uncertainties according to their features can achieve a better robust performance.

In this paper, we have investigated the voltage-dependent P-Q reserve capacity (V-PQRC) evaluation method to exploit the robust reserve potential of distribution systems at the TSO-DSO interface. The core features are listed as follows:

1) The concept of V-PQRC is first proposed to extend the PQRC feasible region into a 3-D feasible space considering the voltage deviation limit at the TSO-DSO interface, to ensure that the reserve evaluation can be more reliable and accurate. By treating the V-PQRC model as a constraint for the transmission system operation optimization, the TSO is able to decide the P-Q reserve request to the DSO and the voltage at the TSO-DSO interface, while simultaneously ensuring the operation security of the distribution system after providing P-Q power supports.

2) To enhance the robustness of the V-PQRC evaluation, the uncertainties of DGs and FLs are separately handled according to their characteristics. The DG uncertainty is characterized by a generalized ambiguity set and the FL uncertainty is coped by designing a constrained sliding mode controller (CSMC).

3) A multi-objective optimization model integrating GRCC and CSMC (GRCC-CSMC) is established for the V-PQRC evaluation. Three objectives are included, i.e., P reserve, Q reserve and the voltage deviation limit at the TSO-DSO interface. The robustness of the obtained P-Q reserve schemes is achieved by introducing both the ambiguity set and CSMC validity constraints into the optimization model.

4) The non-approximated selecting (NAS) method is proposed to build up a simplified V-PQRC linear model with a significantly reduced complexity, so that the model is easy to be applied in the practical T-D system coordinated operation.

The rest of this paper is organized as follows. Section II outlines the reserve potential of distribution systems. Section III proposes the approaches to handle DG and FL uncertainties. Section IV formulates the GRCC-CSMC multi-objective optimization model for the V-PQRC evaluation. The NAS method is proposed in Section V. In Section VI, simulation results are demonstrated. Section VII concludes this paper.

II. Reserve Potential Analysis of Distribution Systems

A. Reserve Feasibility of Distribution Systems

DGs and FLs enable the DSO to provide upward/downward P reserves and inductive/capacitive Q reserves to the transmission system via the TSO-DSO interface. The feasibility is discussed based on a typical radial distribution system, shown in Fig. 1. Upward P reserve ($P_{\rm res} > 0$) and inductive Q reserve ($Q_{\rm res} > 0$) refer to the ability to increase the active and reactive exchange power from the TSO respectively.

The bus voltage deviation inside the distribution system, after providing P or Q power support, is formulated by (1) and (2), respectively. The maximal P and Q power supports that the DSO can provide are regarded as the P and Q reserve capacities. The relationship between reserve capacities and response power of DGs and FLs are derived from (1)–(2), expressed by (3) and (4). The voltage deviation at each bus is limited by (5), for maintaining the voltage security.

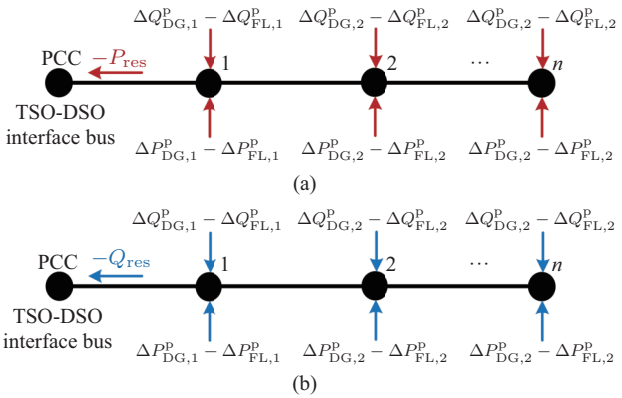

Fig. 1. Illustration of the distribution system with DGs and FLs (each line section connecting bus i and i+1 has the same resistance R and reactance X). (a) P reserve ($P_{\rm res}$) provision (upward: $P_{\rm res}>0$, downward: $P_{\rm res}<0$). (b) Q reserve ($Q_{\rm res}$) provision (inductive: $Q_{\rm res}>0$, capacitive: $Q_{\rm res}<0$).

$$\Delta V^{\rm p}_m=\Delta V_{\rm PCC}-mR\left(P_{\rm res}+\frac{X}{R}\Delta Q^{\rm p}_{\rm PCC}\right)+\sum_{i=1}^{m-1}\Delta L^{\rm p}_i +R\sum_{i=1}^{m-1}\left[(\Delta P^{\rm p}_{{\rm FL},i}-\Delta P^{\rm p}_{{\rm DG},i})+\frac{X}{R}(\Delta Q^{\rm p}_{{\rm FL},i}-\Delta Q^{\rm p}_{{\rm DG},i})\right] \quad m=2,\cdots,n \tag{1}$$

$$\Delta V^{\rm q}_m=\Delta V_{\rm PCC}-mQ_{\rm res}X+\sum_{i=1}^{m-1}\Delta L^{\rm q}_i +R\sum_{i=1}^{m-1}\left[(\Delta P^{\rm q}_{{\rm FL},i}-\Delta P^{\rm q}_{{\rm DG},i})+\frac{X}{R}(\Delta Q^{\rm q}_{{\rm FL},i}-\Delta Q^{\rm q}_{{\rm DG},i})\right] \quad m=2,\cdots,n \tag{2}$$

$$P_{\rm res}=\sum_{m=1}^{n-1}\frac{n-m}{n}(\Delta P^{\rm p}_{{\rm FL},m}-\Delta P^{\rm p}_{{\rm DG},m}) +\frac{X}{R}\sum_{m=1}^{n-1}\frac{n-m}{n}(\Delta Q^{\rm p}_{{\rm FL},m}-\Delta Q^{\rm p}_{{\rm DG},m}) -\frac{X}{R}\Delta Q^{\rm p}_{\rm PCC}+\sum_{m=1}^{n-1}\Delta L^{\rm p}_m+\frac{\Delta V_{\rm PCC}-\Delta V^{\rm p}_n}{nR} \tag{3}$$

$$Q_{\rm res}=\sum_{m=1}^{n-1}\frac{n-m}{n}(\Delta Q^{\rm q}_{{\rm FL},m}-\Delta Q^{\rm q}_{{\rm DG},m}) +\frac{R}{X}\sum_{m=1}^{n-1}\frac{n-m}{n}(\Delta P^{\rm q}_{{\rm FL},m}-\Delta P^{\rm q}_{{\rm DG},m}) +\sum_{m=1}^{n-1}\Delta L^{\rm q}_m+\frac{\Delta V_{\rm PCC}-\Delta V^{\rm q}_n}{nX} \tag{4}$$

$$\Delta\underline{V}_m\le\Delta V_m\le\Delta\overline{V}_m,\ \ m=1,\cdots,n \tag{5}$$

where ΔV_m with superscript p or q are the voltage deviation at bus m after providing P or Q power support respectively; $\Delta V_{\rm PCC}$ is the voltage deviation at the TSO-DSO interface after the DSO provides P or Q power support; $\Delta Q^{\rm p}_{\rm PCC}$ is the reactive exchange power deviation at the TSO-DSO interface due to the P power support; $\Delta P_{{\rm DG},i}$ and $\Delta Q_{{\rm DG},i}$ with superscript p or q represent the active and reactive response power of DGs at bus i to provide P or Q reserves, respectively; $\Delta P_{{\rm FL},i}$ and $\Delta Q_{{\rm FL},i}$ with superscript p or q represent the aggregated active and reactive response power of FLs at bus i to provide P or Q reserves, respectively; $\Delta L^{\rm p}_m$ and $\Delta L^{\rm q}_m$ are the power loss at bus m, due to the P or Q power support; $\Delta\underline{V}_m$ and $\Delta\overline{V}_m$ are the lower and upper limit of the voltage deviation at bus m, respectively.

1) P reserve provision feasibility: it is revealed by (3) that the P reserve ($P_{\rm res}$) is determined by both active and reactive response power of DGs and FLs. With R/X ratios larger than 1, the active response power of DGs and FLs assumes the main role to provide the P reserve. In addition, the influence of DGs and FLs on $P_{\rm res}$ is proportional to their electricity distance from the TSO-DSO interface, that means controlling the DGs and FLs closer to the TSO-DSO interface can achieve a larger P reserve.

2) Q reserve provision feasibility: according to (4), the high R/X ratios also increase the influence of active response power of DGs and FLs on the Q reserve capacity ($Q_{\rm res}$). Controlling the DGs and FLs located as close as possible to the TSO-DSO interface can achieve a larger $Q_{\rm res}$ than controlling the resources further from it. It must be mentioned that the active exchange power should be fixed when the DSO provides the Q power support, because the V-Q control of transmission systems does not change the active power state.

3) Influence of $\Delta V_{\rm PCC}$ on P and Q reserves: it is implied by (3)–(4) that $P_{\rm res}$ and $Q_{\rm res}$ are monotonically increasing according to the difference in voltage between the TSO-DSO interface bus and the end bus. According to (5), $P_{\rm res}$ and $Q_{\rm res}$ can reach maximum values when the voltage difference is up to $\Delta V_{\rm PCC}-\Delta\underline{V}_n$, and reach minimum values when the voltage difference is down to $\Delta V_{\rm PCC}-\Delta\overline{V}_n$. Therefore, $\Delta V_{\rm PCC}$ directly influences the feasible range of $P_{\rm res}$ and $Q_{\rm res}$. However, $\Delta V_{\rm PCC}$ is unknown for the DSO because it is usually determined by the TSO. Therefore, it is practical to consider the voltage deviation limit at the TSO-DSO interface ($\Delta V^*_{\rm PCC}$) so that the DSO can tolerate the operation security in the reserve evaluation.

Figure 2 presents an equivalent T-D system studied in this paper, where an IEEE-33 bus distribution system is connected to the bus 97 of the IEEE-118 bus transmission system.

B. Challenges for the Reserve Provision

1) Voltage security. According to (1) and (2), the bus voltage inside the distribution system is determined by $\Delta V_{\rm PCC}$ and the response power at each bus. Moreover, the high R/X ratios cause the bus voltage to be sensitive to both the active and reactive response power of DGs and FLs. Therefore, the voltage security should be satisfied in the reserve evaluation, with the consideration of $\Delta V^*_{\rm PCC}$.

2) The uncertainties of DGs and FLs. The DG response power can be controlled by changing its setpoint. However, due to its intermittent nature, the DG actual response power ($\Delta P_{{\rm DG},i}$) may deviate from the desired value ($\Delta P^{\rm d}_{{\rm DG},i}$), formulated by (6).

$$\Delta P_{{\rm DG},i}=\Delta P^{\rm d}_{{\rm DG},i}+\omega_{{\rm DG},i} \tag{6}$$

where the superscript d represents the desired value from the DSO; $\omega_{{\rm DG},i}$ is the forecasting error, i.e., DG uncertainty.

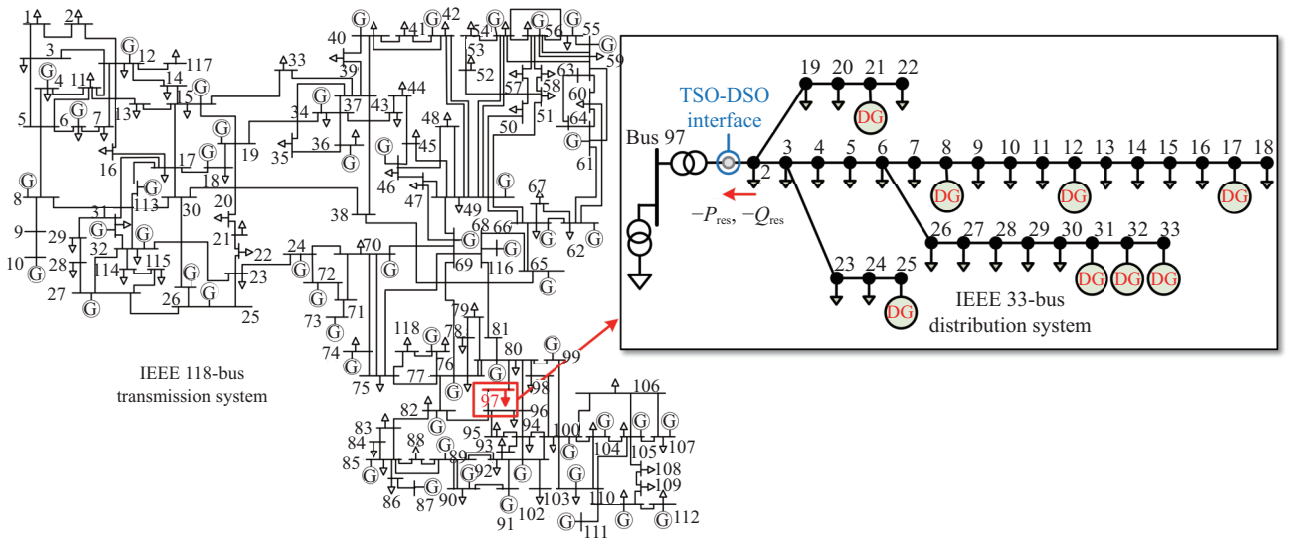

Fig. 2. Illustration of the T-D system.

The DG uncertainty usually comes from the sudden change of weather. The output power of wind or photovoltaic power generation will deviate from the setpoint when the wind speed changes or a cloud moves. It is hard to accurately predict the sudden change. Such uncertainty may disturb the reserve evaluation and affect the distribution system operation security.

The FL uncertainty primarily results from the contracted individuals refusing or interrupting response [26], which will deviate the FL response power from its desired value. The FLs connecting to the same bus, such as residential air conditioning and electric vehicles, are commonly managed together. The aggregated FL response power at bus i can be expressed by (7).

$$\Delta P_{{\rm FL},i} = \frac{1}{1+sT_{{\rm FL},i}}(\Delta u_{{\rm FL},i} + \omega_{{\rm FL},i}) \tag{7}$$

$$\Delta P_{{\rm FL},i}^{\rm down} \le \Delta u_{{\rm FL}.i} \le \Delta P_{{\rm FL},i}^{\rm up} \tag{8}$$

where $\Delta u_{{\rm FL},i}$ is the control signal for FLs at bus i, which is bounded by (8) due to the FL response willingness; $\Delta P_{{\rm FL},i}^{\rm down}$ and $\Delta P_{{\rm FL},i}^{\rm up}$ are downward and upward limits for $\Delta u_{{\rm FL},i}$ respectively; $\omega_{{\rm FL},i}$ is the aggregated FL uncertainty; $T_{{\rm FL},i}$ is the FL response time, which is a random value affected by the communication and control links. In practice, the value must be within the limit from DSO or TSO, such as 4 s used by California ISO [27].

Since the FL uncertainty of each individual occurs along the response process, the aggregated FL uncertainty ($\omega_{{\rm FL},i}$) is time changing. As a result, the aggregated FL response power ($\Delta P_{{\rm FL},i}$) may fluctuate over the whole dispatch interval, which threatens the reliability of the reserve evaluation.

3) Resource conflict risk. As mentioned before, the DGs and FLs are controlled by the DSO to provide both P and Q reserves. Therefore, it is necessary to coordinately evaluate the P and Q reserve capacity (PQRC) in practice.

C. Introduction of the V-PQRC

The V-PQRC is introduced in this paper to formulate a 3-D feasible space for PQRC, with the consideration of the voltage deviation limit ($\Delta V_{\rm PCC}^*$) at the TSO-DSO interface. Within the feasible space, the DSO can reliably provide $P_{\rm res}$ and $Q_{\rm res}$ when the voltage deviation at the TSO-DSO interface is kept within its limit. After providing the P-Q power support, the distribution system security constraints ($\boldsymbol{\Phi}$) will also be satisfied under the uncertainties of DGs and FLs. The mathematical expression of V-PQRC ($\boldsymbol{\Gamma}_{\rm res}$) is formulated as:

$$\begin{aligned}\boldsymbol{\Gamma}_{\rm res} = \{&P_{\rm res}, Q_{\rm res}, \Delta V_{\rm PCC}^* : \forall \boldsymbol{\omega}_{\rm DG}, \boldsymbol{\omega}_{\rm FL},\\ &\exists \boldsymbol{x}, (\boldsymbol{x}, \Delta V_{\rm PCC}^*) \in \boldsymbol{\Phi}\}\end{aligned} \tag{9}$$

where $\boldsymbol{x}$ is the decision variable vector consisting of the desired response power of DGs and FLs for re-dispatching, providing P reserve and Q reserve, $\boldsymbol{x} = [\Delta \boldsymbol{P}_{\rm DG}^{\rm d,r/p/q}, \Delta \boldsymbol{Q}_{\rm DG}^{\rm d,r/p/q}, \Delta \boldsymbol{P}_{\rm FL}^{\rm d,r/p/q}]$; Superscript r represents the re-dispatching process, at which the DSO can reset the operating point of DGs and FLs in advance to preserve more response capacity for P and Q reserves.

From the aspect of the TSO, the V-PQRC reveals the permitted range of $\Delta V_{\rm PCC}^*$ for the distribution system operation security, as well as the relationship between $\Delta V_{\rm PCC}^*$ and the feasible PQRC of the distribution system. It causes the T-D system coordination to be more efficient, as illustrated in Fig. 3.

At the beginning of the dispatch interval, the DSO evaluates and sends the V-PQRC model to the TSO. The V-PQRC model enables the TSO to utilize the distribution system as a virtual voltage-dependent P-Q reserve resource at the TSO-DSO interface. By taking the V-PQRC model as a constraint in the transmission system operation optimization, the TSO is able to determine the P-Q reserve requests and the value of $\Delta V_{\rm PCC}^*$. Then, the DSO redispatches and allocates the reserve requests among DGs and FLs. During the interval, if frequency or voltage regulation problems occur, the TSO can issue the P or Q power support command to the DSO. The DSO will control its internal resources to respond to the TSO's command, according to the reserve allocation. Therefore, the transmission system operation can be facilitated by exploiting the reserve ability of distribution systems.

According to Fig. 3, the V-PQRC model-based T-D system coordination can be conducted efficiently without iterative interaction between TSO and DSO.

D. Outlines for V-PQRC Evaluation

The procedure to evaluate and formulate the V-PQRC model is outlined in Fig. 4. First, a generalized ambiguity set is modeled to cover the possible distribution of DG uncertainty. The CSMC is designed to smooth the influence of aggregated FL uncertainty on the response of FLs. Then, the GRCC-CSMC multi-objective optimization model is established for V-PQRC evaluation and solved by the NSGA-II algorithm. The DG generalized ambiguity set and the validity constraint of CSMC are introduced into the optimization as constraints, so that the obtained Pareto optimal solutions can also achieve a well robust performance under uncertainties of both DGs and FLs. Finally, the NAS method is proposed to generate a V-PQRC linear model to facilitate the transmission system decision-making.

It should be noted that the resources that have been involved in the distribution system V-Q control are not considered again for the V-PQRC evaluation, such as capacitors, SVC/SVG and OTLC. Thus, the distribution system V-Q control will not be affected by the P-Q reserve provision for the transmission system.

III. Approaches to Handle the DG Uncertainty and FL Uncertainty

A. Generalized Ambiguity Set for the DG Uncertainty

Since the DG uncertainty cannot be accurately predicted and the historical data can be inadequate in some circumstances, a generalized ambiguity set $\boldsymbol{U}_{\mathrm{DG}}$ (10) is established to capture the possible joint distributions of the uncertainty of all available DGs, depending on the estimated mean vector ($\boldsymbol{\theta}_{\mathrm{DG}}$) and the estimated covariance matrix ($\boldsymbol{\Sigma}_{\mathrm{DG}}$).

$$\boldsymbol{U}_{\mathrm{DG}} = \begin{cases} \int f(\boldsymbol{\omega}_{\mathrm{DG}})\mathrm{d}\boldsymbol{\omega}_{\mathrm{DG}} = 1, f(\boldsymbol{\omega}_{\mathrm{DG}}) \geq 0 \\ [\mathrm{E}(\boldsymbol{\omega}_{\mathrm{DG}}) - \boldsymbol{\theta}_{\mathrm{DG}}]^{\mathrm{T}} \boldsymbol{\Sigma}_{\mathrm{DG}}^{-1} [\mathrm{E}(\boldsymbol{\omega}_{\mathrm{DG}}) - \boldsymbol{\theta}_{\mathrm{DG}}] \leq \gamma_1 \\ \mathrm{E}[(\boldsymbol{\omega}_{\mathrm{DG}} - \boldsymbol{\theta}_{\mathrm{DG}})(\boldsymbol{\omega}_{\mathrm{DG}} - \boldsymbol{\theta}_{\mathrm{DG}})^{\mathrm{T}}] \prec \gamma_2 \boldsymbol{\Sigma}_{\mathrm{DG}} \end{cases} \tag{10}$$

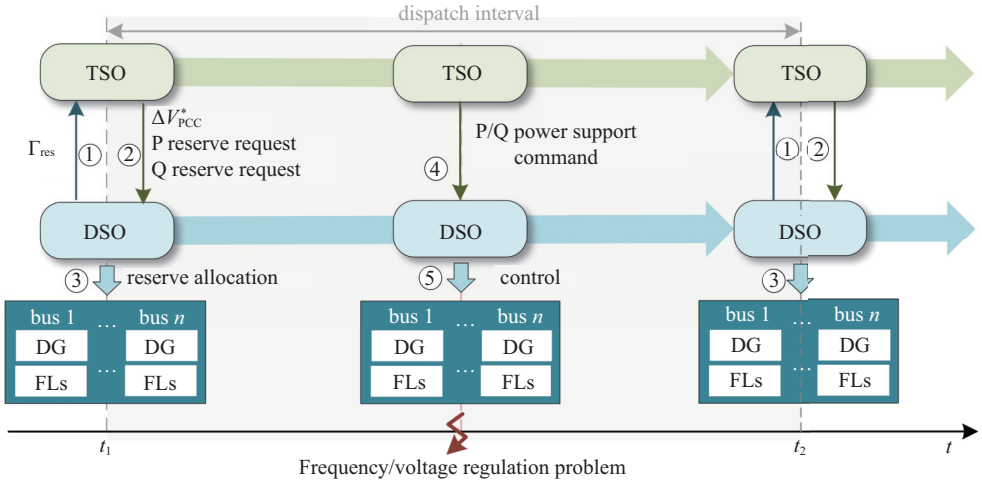

Fig. 3. Illustration of the V-PQRC model-based T-D interaction.

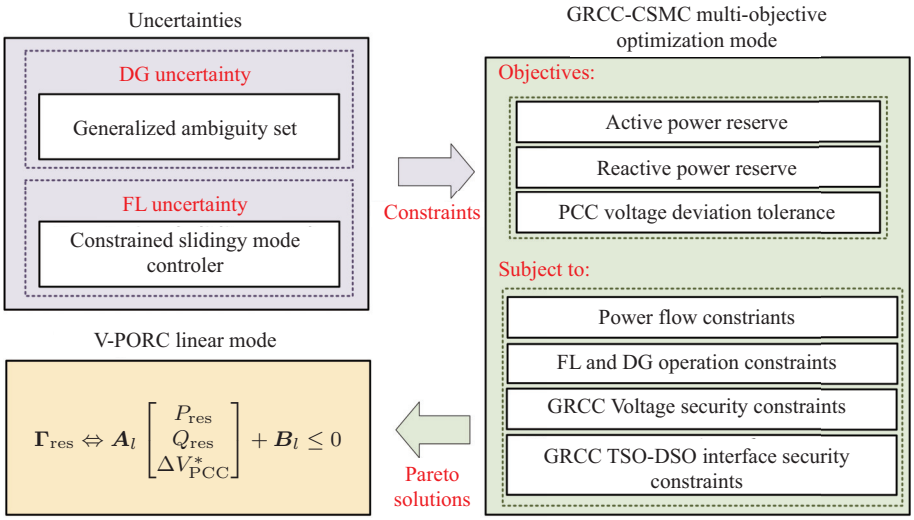

Fig. 4. Outline of the V-PQRC evaluation and modelling procedure.

where $f(\boldsymbol{\omega}_{\mathrm{DG}})$ is the joint probability distribution; γ_1 and γ_2 are parameters reflecting the decision-maker's confidence in the empirical estimates $\boldsymbol{\theta}_{\mathrm{DG}}$, $\boldsymbol{\Sigma}_{\mathrm{DG}}$ respectively, $\gamma_1 \geq 0$ and $\gamma_2 \geq 1$.

The generalized ambiguity set can be considered as a generalization form of many moment-based ambiguity sets [22]. It has been proved to be effectively conservative and robust in the case of inadequate historical data [17].

When there is enough historical data, the generalized ambiguity set can be less conservative by changing γ_1, γ_2, $\boldsymbol{\theta}_{\mathrm{DG}}$, $\boldsymbol{\Sigma}_{\mathrm{DG}}$, or strengthening inner constraints [23]. In both cases, the proposed V-PQRC evaluation method can still be valid.

B. Constrained Sliding Mode Controller for the FL Uncertainty

It is possible to smooth the aggregated FL uncertainty ($\omega_{\mathrm{FL},i}$) at bus i within the aggregation. For instance, if one FL suddenly stops responding, another available FL can be controlled to respond as a substitute, so that the aggregated response power ($\Delta P_{\mathrm{FL},i}$) will not be obviously disturbed.

Inspired by our previous study in [26], a constrained sliding mode controller (CSMC) is designed to drive the aggregated response power to track the desired value $\Delta P^{\mathrm{d}}_{\mathrm{FL},i}$, by using the control signal ($\Delta u_{\mathrm{FL},i}$) constrained via (8) as the input.

The response error is chosen as the sliding variable $s_{\mathrm{FL},i}$:

$$s_{\mathrm{FL},i} = \Delta P_{\mathrm{FL},i} - \Delta P^{\mathrm{d}}_{\mathrm{FL},i} \tag{11}$$

According to (11), $\Delta P_{\mathrm{FL},i}$ will not be influenced by the FL uncertainty when the sliding surface $s_{\mathrm{FL},i} = 0$ is reached. Based on (7) and (11), a power function-based sliding mode control law is designed to make the sliding surface reachable:

$$\Delta u_{\mathrm{FL},i} = \Delta P^{\mathrm{d}}_{\mathrm{FL},i} - k_{\mathrm{FL},i}|s_{\mathrm{FL},i}|^{1/2}\,\mathrm{sgn}(s_{\mathrm{FL},i}) \tag{12}$$

where $k_{\mathrm{FL},i}$ is a pre-determined positive constant; the function $\mathrm{sgn}(s_{\mathrm{FL},i})$ is formulated as:

$$\mathrm{sgn}(s_{\mathrm{FL},i}) = \begin{cases} 1, & s_{\mathrm{FL},i} > 0 \\ 0, & s_{\mathrm{FL},i} = 0 \\ -1, & s_{\mathrm{FL},i} < 0 \end{cases}$$

Since the control signal $\Delta u_{\mathrm{FL},i}$ is constrained by (8), the CSMC is valid only if the reachability of the sliding surface is ensured under this constraint. So, theorem 1 for CSMC is proposed to ensure the validity of CSMC.

Theorem 1. if $\Delta u_{\mathrm{FL},i}$ is bounded by (8) and $\|\omega_{\mathrm{FL},i}\| \leq \overline{\omega}_{\mathrm{FL},i}$ exists, where $\overline{\omega}_{\mathrm{FL},i}$ is a pre-known positive constant, the sliding surface can be reached in finite time under the sliding control law (12), when $\Delta P^{\mathrm{d}}_{\mathrm{FL},i}$ is constrained by:

$$\Delta P^{\mathrm{down}}_{\mathrm{FL},i} + \bar{\omega}_{\mathrm{FL},i} \leq \Delta P^{\mathrm{d}}_{\mathrm{FL},i} \leq \Delta P^{\mathrm{up}}_{\mathrm{FL},i} - \bar{\omega}_{\mathrm{FL},i} \tag{13}$$

Theorem 1 is proved by the Lyapunov method [28]–[30], which is discussed in Appendix A. The aggregated FL response power under CSMC is illustrated by Fig. 5.

It is clear that the aggregated response power can track the desired value when the constraint (13) is met, and fails when the constraint is broken. Therefore, the robustness of the V-PQRC evaluation under the FL uncertainty can be enhanced by using the CSMC and satisfying the CSMC validity constraint (13).

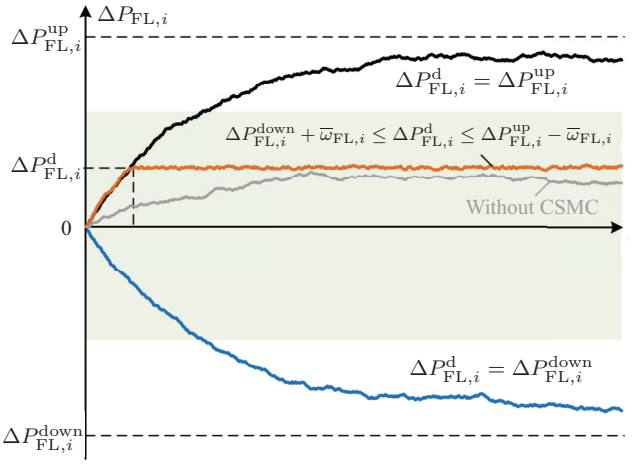

Fig. 5. Illustration of the aggregated FL response power under CSMC.

The control signal ($\Delta u_{\mathrm{FL},i}$) can be allocated to individuals via centralized or decentralized approaches [31], [32]. Since it is not the focus in this paper, the allocation is not further studied here.

IV. Multi-Objective Optimization Model Integrating GRCC and CSMC for V-PQRC Evaluation

A. Objectives

In the V-PQRC evaluation, we are concerned with three objectives: 1) how much upward or downward P reserve can be provided, formulated by (14); 2) how much inductive or capacitive Q reserve can be provided in addition to the P reserves, formulated by (15); 3) the voltage deviation limit at the TSO-DSO interface for the distribution system operation security, formulated by (16).

1) P reserve capacity objective F_1

$$\max F_1 = \eta_1 P_{\mathrm{res}} \tag{14}$$

where η_1 is a constant value 1 or -1, to represent the upward P reserve or downward P reserve, respectively.

2) Reactive power reserve capacity objective F_2

$$\max F_2 = \eta_2 Q_{\mathrm{res}} \tag{15}$$

where η_2 is a constant value 1 or -1, to represent the inductive Q reserve or capacitive Q reserve, respectively.

3) Voltage deviation limit F_3 at TSO-DSO interface

$$\max F_3 = \eta_3 \Delta V^{*}_{\mathrm{PCC}} \tag{16}$$

where η_3 is a constant value 1 or -1, to represent the upper or lower limit of the voltage deviation at the TSO-DSO interface for the system operation security, respectively.

Considering that the market mechanisms for the P-Q reserve services of distribution systems are not yet mature, the market-related and cost-related elements are not considered in the above objectives. However, the V-PQRC evaluation method is still valid when further considering these elements.

B. Deterministic Constraints

1) Linearized Power Flow Constraints

The power flow model is linearized around the initial operation point at the beginning of the dispatch interval, based on the sensitivities of state variables (voltage, P reserve, Q reserve, etc.) regarding the decision variables $\boldsymbol{x}$ and $\Delta V^{*}_{\mathrm{PCC}}$.

The linearized power flow models of the distribution system for re-dispatching, providing P and Q reserves are formulated by (17)–(20). The TSO-DSO interface is assumed as the slack bus for the calculation request. Moreover, $\Delta V^{*}_{\mathrm{PCC}}$ is considered when calculating the bus voltage deviation due to the P or Q power support for TSO, formulated as (18).

$$\Delta \boldsymbol{V}^{\mathrm{r}} = \boldsymbol{S}_{\mathrm{V-P}} \begin{bmatrix} -\Delta \boldsymbol{P}^{\mathrm{d,r}}_{\mathrm{DG}} \\ \Delta \boldsymbol{P}^{\mathrm{d,r}}_{\mathrm{FL}} \end{bmatrix} + \boldsymbol{S}_{\mathrm{V-Q}} \begin{bmatrix} -\Delta \boldsymbol{Q}^{\mathrm{d,r}}_{\mathrm{DG}} \\ \cot \boldsymbol{\varphi} \cdot \Delta \boldsymbol{P}^{\mathrm{d,r}}_{\mathrm{FL}} \end{bmatrix} \tag{17}$$

$$\Delta \boldsymbol{V}^{\mathrm{p/q}} = \boldsymbol{S}_{\mathrm{V-P}} \begin{bmatrix} -\Delta \boldsymbol{P}^{\mathrm{d,p/q}}_{\mathrm{DG}} \\ \Delta \boldsymbol{P}^{\mathrm{d,p/q}}_{\mathrm{FL}} \end{bmatrix} + \boldsymbol{S}_{\mathrm{V-Q}} \begin{bmatrix} -\Delta \boldsymbol{Q}^{\mathrm{d,p/q}}_{\mathrm{DG}} \\ \cot \boldsymbol{\varphi} \cdot \Delta \boldsymbol{P}^{\mathrm{d,p/q}}_{\mathrm{FL}} \end{bmatrix} + S_{\mathrm{V-V}} \Delta V^{*}_{\mathrm{PCC}} \tag{18}$$

$$\Delta P^{\mathrm{r/p/q}}_{\mathrm{PCC}} = \boldsymbol{S}^{\mathrm{T}}_{\mathrm{P-P}} \begin{bmatrix} -\Delta \boldsymbol{P}^{\mathrm{d,r/p/q}}_{\mathrm{DG}} \\ \Delta \boldsymbol{P}^{\mathrm{d,r/p/q}}_{\mathrm{FL}} \end{bmatrix} + \boldsymbol{S}^{\mathrm{T}}_{\mathrm{P-Q}} \begin{bmatrix} -\Delta \boldsymbol{Q}^{\mathrm{d,r/p/q}}_{\mathrm{DG}} \\ \cot \boldsymbol{\varphi} \cdot \Delta \boldsymbol{P}^{\mathrm{d,r/p/q}}_{\mathrm{FL}} \end{bmatrix} \tag{19}$$

$$\Delta Q^{\mathrm{r/p/q}}_{\mathrm{PCC}} = \boldsymbol{S}^{\mathrm{T}}_{\mathrm{Q-P}} \begin{bmatrix} -\Delta \boldsymbol{P}^{\mathrm{d,r/p/q}}_{\mathrm{DG}} \\ \Delta \boldsymbol{P}^{\mathrm{d,r/p/q}}_{\mathrm{FL}} \end{bmatrix} + \boldsymbol{S}^{\mathrm{T}}_{\mathrm{Q-Q}} \begin{bmatrix} -\Delta \boldsymbol{Q}^{\mathrm{d,r/p/q}}_{\mathrm{DG}} \\ \cot \boldsymbol{\varphi} \cdot \Delta \boldsymbol{P}^{\mathrm{d,r/p/q}}_{\mathrm{FL}} \end{bmatrix} \tag{20}$$

where $\boldsymbol{\Delta V}$ with superscript r, p/q are the bus voltage deviation vectors caused by the re-dispatching, P/Q power support respectively; ΔP_{PCC} and ΔQ_{PCC} with superscript r, p/q are the active and reactive exchange power deviation caused by re-dispatching, P/Q power support, respectively; $\boldsymbol{S}_{\mathrm{V-P}}$, $\boldsymbol{S}_{\mathrm{P-P}}$, $\boldsymbol{S}_{\mathrm{Q-P}}$ are the voltage sensitivity matrix, active exchange power sensitivity vector, reactive exchange power sensitivity vector around the active power load at each bus, respectively; $\boldsymbol{S}_{\mathrm{V-Q}}$, $\boldsymbol{S}_{\mathrm{P-Q}}$, $\boldsymbol{S}_{\mathrm{P-Q}}$ are the voltage sensitivity matrix, active exchange power sensitivity vector, reactive exchange power sensitivity vector around the reactive power load at each bus, respectively; $\boldsymbol{S}_{\mathrm{V-V}}$ is the voltage sensitivity vector around the voltage at the TSO-DSO interface; $\boldsymbol{\varphi}$ is the power factor angle vector of FLs.

The P reserve capacity (P_{res}) and Q reserve capacity (Q_{res}) are equivalent to $\Delta P^{\mathrm{p}}_{\mathrm{PCC}}$ and $\Delta P^{\mathrm{q}}_{\mathrm{PCC}}$, respectively. Considering that the active exchange power should be fixed when providing the Q power support, additional constraint (21) is formulated.

$$\Delta P^{\mathrm{q}}_{\mathrm{PCC}} = \boldsymbol{S}^{\mathrm{T}}_{\mathrm{P-P}} \begin{bmatrix} -\Delta \boldsymbol{P}^{\mathrm{d,q}}_{\mathrm{DG}} \\ \Delta \boldsymbol{P}^{\mathrm{d,q}}_{\mathrm{FL}} \end{bmatrix} + \boldsymbol{S}^{\mathrm{T}}_{\mathrm{P-Q}} \begin{bmatrix} -\Delta \boldsymbol{Q}^{\mathrm{d,q}}_{\mathrm{DG}} \\ \cot \boldsymbol{\varphi} \cdot \Delta \boldsymbol{P}^{\mathrm{d,q}}_{\mathrm{FL}} \end{bmatrix} = 0 \tag{21}$$

2) FL Operation Constraints Under CSMC

The CSMC validity constraint (13) is utilized to restrict the FL operation, so that the desired response power can be realized by CSMC regardless of the FL uncertainty. According to (13), the desired aggregate FL response power for re-dispatching, providing P and Q reserves are bounded by:

$$\Delta \boldsymbol{P}^{\mathrm{down}}_{\mathrm{FL}} + \overline{\boldsymbol{\omega}}_{\mathrm{FL}} \le \Delta \boldsymbol{P}^{\mathrm{d,r}}_{\mathrm{FL}} \le \Delta \boldsymbol{P}^{\mathrm{up}}_{\mathrm{FL}} - \overline{\boldsymbol{\omega}}_{\mathrm{FL}} \tag{22a}$$

$$\max \begin{Bmatrix} \Delta \boldsymbol{P}^{\mathrm{down}}_{\mathrm{FL}} + \overline{\boldsymbol{\omega}}_{\mathrm{FLA}}, \Delta \boldsymbol{P}^{\mathrm{down}}_{\mathrm{FL}} + \overline{\boldsymbol{\omega}}_{\mathrm{FL}} - \Delta \boldsymbol{P}^{\mathrm{d,r}}_{\mathrm{FL}}, \\ \Delta \boldsymbol{P}^{\mathrm{down}}_{\mathrm{FL}} + \overline{\boldsymbol{\omega}}_{\mathrm{FL}} - \Delta \boldsymbol{P}^{\mathrm{d,r}}_{\mathrm{FL}} - \Delta \boldsymbol{P}^{\mathrm{d,q}}_{\mathrm{FL}} \end{Bmatrix} \le \Delta \boldsymbol{P}^{\mathrm{d,p}}_{\mathrm{FL}} \le \min \begin{Bmatrix} \Delta \boldsymbol{P}^{\mathrm{up}}_{\mathrm{FL}} - \overline{\boldsymbol{\omega}}_{\mathrm{FL}}, \Delta \boldsymbol{P}^{\mathrm{up}}_{\mathrm{FL}} - \overline{\boldsymbol{\omega}}_{\mathrm{FL}} - \Delta \boldsymbol{P}^{\mathrm{d,r}}_{\mathrm{FL}}, \\ \Delta \boldsymbol{P}^{\mathrm{up}}_{\mathrm{FL}} - \overline{\boldsymbol{\omega}}_{\mathrm{FL}} - \Delta \boldsymbol{P}^{\mathrm{d,r}}_{\mathrm{FL}} - \Delta \boldsymbol{P}^{\mathrm{d,q}}_{\mathrm{FL}} \end{Bmatrix} \tag{22b}$$

$$\max \begin{Bmatrix} \Delta \boldsymbol{P}^{\mathrm{down}}_{\mathrm{FL}} + \overline{\boldsymbol{\omega}}_{\mathrm{FL}}, \Delta \boldsymbol{P}^{\mathrm{down}}_{\mathrm{FL}} + \overline{\boldsymbol{\omega}}_{\mathrm{FL}} - \Delta \boldsymbol{P}^{\mathrm{d,r}}_{\mathrm{FL}}, \\ \Delta \boldsymbol{P}^{\mathrm{down}}_{\mathrm{FL}} + \overline{\boldsymbol{\omega}}_{\mathrm{FL}} - \Delta \boldsymbol{P}^{\mathrm{d,r}}_{\mathrm{FL}} - \Delta \boldsymbol{P}^{\mathrm{d,p}}_{\mathrm{FL}} \end{Bmatrix} \le \Delta \boldsymbol{P}^{\mathrm{d,q}}_{\mathrm{FL}} \le \min \begin{Bmatrix} \Delta \boldsymbol{P}^{\mathrm{up}}_{\mathrm{FL}} - \overline{\boldsymbol{\omega}}_{\mathrm{FL}}, \Delta \boldsymbol{P}^{\mathrm{up}}_{\mathrm{FL}} - \overline{\boldsymbol{\omega}}_{\mathrm{FL}} - \Delta \boldsymbol{P}^{\mathrm{d,r}}_{\mathrm{FL}}, \\ \Delta \boldsymbol{P}^{\mathrm{up}}_{\mathrm{FL}} - \overline{\boldsymbol{\omega}}_{\mathrm{FL}} - \Delta \boldsymbol{P}^{\mathrm{d,r}}_{\mathrm{FL}} - \Delta \boldsymbol{P}^{\mathrm{d,p}}_{\mathrm{FL}} \end{Bmatrix} \tag{22c}$$

3) DG Operation Constraints

The DG converter is assumed to operate under the P-Q control mode. The initial DG active output power ($\boldsymbol{P}^{(0)}_{\mathrm{DG}}$) is set at the optimal operating point of the MPPT curve, so that the active output power cannot exceed the initial value. Based on it, DG active response power constraints are formulated by (23).

$$\begin{cases} -\boldsymbol{P}^{(0)}_{\mathrm{DG}} \cdot \rho_{\mathrm{curt}} \le \Delta \boldsymbol{P}^{\mathrm{d,r}}_{\mathrm{DG}} \le \boldsymbol{0} \\ -\boldsymbol{P}^{(0)}_{\mathrm{DG}} \le \Delta \boldsymbol{P}^{\mathrm{d,r}}_{\mathrm{DG}} + \Delta \boldsymbol{P}^{\mathrm{d,p/q}}_{\mathrm{DG}} \le \boldsymbol{0} \\ -\boldsymbol{P}^{(0)}_{\mathrm{DG}} \le \Delta \boldsymbol{P}^{\mathrm{d,r}}_{\mathrm{DG}} + \Delta \boldsymbol{P}^{\mathrm{d,p}}_{\mathrm{DG}} + \Delta \boldsymbol{P}^{\mathrm{d,q}}_{\mathrm{DG}} \le \boldsymbol{0} \end{cases} \tag{23}$$

where ρ_{curt} is the permitted curtailment ratio to ensure the DG penetration up to the minimal requirement. DGs are allowed to curtail all the active output power to provide power supports.

The DG capacity constraints are formulated by (24a)–(24c).

$$\left(P^{(0)}_{\mathrm{DG},i} + \Delta P^{\mathrm{d,r}}_{\mathrm{DG},i}\right)^2 + \left(Q^{(0)}_{\mathrm{DG},i} + \Delta Q^{\mathrm{d,r}}_{\mathrm{DG},i}\right)^2 \le S^2_{\mathrm{DG},i} \tag{24a}$$

$$\left(P^{(0)}_{\mathrm{DG},i} + \Delta P^{\mathrm{d,r}}_{\mathrm{DG},i} + \Delta P^{\mathrm{d,p/q}}_{\mathrm{DG},i}\right)^2 + \left(Q^{(0)}_{\mathrm{DG},i} + \Delta Q^{\mathrm{d,r}}_{\mathrm{DG},i} + \Delta Q^{\mathrm{d,p/q}}_{\mathrm{DG},i}\right)^2 \le S^2_{\mathrm{DG},i} \tag{24b}$$

$$\left(P^{(0)}_{\mathrm{DG},i} + \Delta P^{\mathrm{d,r}}_{\mathrm{DG},i} + \Delta P^{\mathrm{d,p}}_{\mathrm{DG},i} + \Delta P^{\mathrm{d,q}}_{\mathrm{DG},i}\right)^2 + \left(Q^{(0)}_{\mathrm{DG},i} + \Delta Q^{\mathrm{d,r}}_{\mathrm{DG},i} + \Delta Q^{\mathrm{d,p}}_{\mathrm{DG},i} + \Delta Q^{\mathrm{d,q}}_{\mathrm{DG},i}\right)^2 \le S^2_{\mathrm{DG},i} \tag{24c}$$

where $S_{\mathrm{DG},i}$ is the DG capacity at bus i; $Q^{(0)}_{\mathrm{DG},i}$ is the initial DG reactive output power at bus i.

The constraints (24a)–(24c) can be linearized by polyhedral approximation [33]. The regular octagon inner-approximation method is utilized in this paper to transfer (24) into (25).

$$\boldsymbol{a}_{\mathrm{oct}}\left(\boldsymbol{P}^{(0)}_{\mathrm{DG}} + \Delta \boldsymbol{P}^{\mathrm{d,r}}_{\mathrm{DG}}\right)^{\mathrm{T}} + \boldsymbol{b}_{\mathrm{oct}}\left(\boldsymbol{Q}^{(0)}_{\mathrm{DG}} + \Delta \boldsymbol{Q}^{\mathrm{d,r}}_{\mathrm{DG}}\right)^{\mathrm{T}} \le \boldsymbol{c}_{\mathrm{oct}} \boldsymbol{S}^{\mathrm{T}}_{\mathrm{DG}} \tag{25a}$$

$$\boldsymbol{a}_{\mathrm{oct}}\left(\boldsymbol{P}^{(0)}_{\mathrm{DG}} + \Delta \boldsymbol{P}^{\mathrm{d,r}}_{\mathrm{DG}} + \Delta \boldsymbol{P}^{\mathrm{d,p/q}}_{\mathrm{DG}}\right)^{\mathrm{T}} + \boldsymbol{b}_{\mathrm{oct}}\left(\boldsymbol{Q}^{(0)}_{\mathrm{DG}} + \Delta \boldsymbol{Q}^{\mathrm{d,r}}_{\mathrm{DG}} + \Delta \boldsymbol{Q}^{\mathrm{d,p/q}}_{\mathrm{DG}}\right)^{\mathrm{T}} \le \boldsymbol{c}_{\mathrm{oct}} \boldsymbol{S}^{\mathrm{T}}_{\mathrm{DG}} \tag{25b}$$

$$\boldsymbol{a}_{\mathrm{oct}}\left(\boldsymbol{P}^{(0)}_{\mathrm{DG}} + \Delta \boldsymbol{P}^{\mathrm{d,r}}_{\mathrm{DG}} + \Delta \boldsymbol{P}^{\mathrm{d,p}}_{\mathrm{DG}} + \Delta \boldsymbol{P}^{\mathrm{d,q}}_{\mathrm{DG}}\right)^{\mathrm{T}} + \boldsymbol{b}_{\mathrm{oct}}\left(\boldsymbol{Q}^{(0)}_{\mathrm{DG}} + \Delta \boldsymbol{Q}^{\mathrm{d,r}}_{\mathrm{DG}} + \Delta \boldsymbol{Q}^{\mathrm{d,p}}_{\mathrm{DG}} + \Delta \boldsymbol{Q}^{\mathrm{d,q}}_{\mathrm{DG}}\right)^{\mathrm{T}} \le \boldsymbol{c}_{\mathrm{oct}} \boldsymbol{S}^{\mathrm{T}}_{\mathrm{DG}} \tag{25c}$$

where $\boldsymbol{S}_{\mathrm{DG}}$ is the DG capacity vector; $\boldsymbol{a}_{\mathrm{oct}}$, $\boldsymbol{b}_{\mathrm{oct}}$ and $\boldsymbol{c}_{\mathrm{oct}}$ are coefficient vectors of the regular octagon inner-approximation.

4) Voltage Security Constraint for Re-dispatching

Since the DSO can measure the actual DG output power at the beginning of the dispatch interval, the operation security constraints for re-dispatching are deterministic.

The bus voltage inside the distribution system should be kept with the limits after re-dispatching, formulated by (26).

$$\underline{\boldsymbol{V}} \le \boldsymbol{V}^{(0)} + \Delta\boldsymbol{V}^{\mathrm{r}} \le \overline{\boldsymbol{V}} \tag{26}$$

where $\underline{\boldsymbol{V}}$ and $\overline{\boldsymbol{V}}$ are the lower and upper limit vectors of voltage security, respectively; $\boldsymbol{V}^{(0)}$ is the initial bus voltage vector.

5) TSO-DSO Interface Security Constraints for Re-dispa- tching

The active exchange power after re-dispatching should meet the power fluctuation constraint and the transmission capacity constraint, formulated by (27) and (28) respectively.

$$\Delta\underline{P}_{\mathrm{PCC}} \le \Delta P_{\mathrm{PCC}} \le \Delta\bar{P}_{\mathrm{PCC}} \tag{27}$$

$$(P^{(0)}_{\mathrm{PCC}} + \Delta P_{\mathrm{PCC}})^2 + (Q^{(0)}_{\mathrm{PCC}} + \Delta Q_{\mathrm{PCC}})^2 \le S^2_{\mathrm{PCC}} \tag{28}$$

where $\Delta\underline{P}_{\mathrm{PCC}}$ and $\Delta\overline{P}_{\mathrm{PCC}}$ are the lower and upper limits of the active exchange power fluctuation, predetermined by TSO and DSO; $P^{(0)}_{\mathrm{PCC}}$ and $Q^{(0)}_{\mathrm{PCC}}$ are the initial active and reactive exchange power, respectively; S_{PCC} is the transmission capacity.

C. Generalized Robust Chance Constraints

Considering that the DG uncertainty over the dispatch interval is inevitable, the generalized robust chance constraints (29) are formulated to ensure that the infimum voltage security probability under the generalized ambiguity set (10) to be at least $(1-\mu_V)$, for three power support situations: providing P or Q power supports; providing P and Q power supports; not providing any power support. The voltage deviation at the TSO-DSO interface after all situations are assumed to reach its limit ($\Delta V^*_{\mathrm{PCC}}$).

$$\begin{cases} \inf\limits_{\boldsymbol{\omega}_{\mathrm{DG}}\in U_{\mathrm{DG}}} \Pr(\boldsymbol{V} \le \{\boldsymbol{V}^{(0)} + \Delta\boldsymbol{V}^{\mathrm{r}} + S_{\mathrm{V-V}}\Delta V^*_{\mathrm{PCC}} \\ \qquad -\boldsymbol{S}^{\mathrm{DG}}_{\mathrm{V-P}}\boldsymbol{\omega}_{\mathrm{DG}}\} \le \overline{\boldsymbol{V}}) \ge 1-\mu_{\mathrm{V}} \\ \inf\limits_{\boldsymbol{\omega}_{\mathrm{DG}}\in U_{\mathrm{DG}}} \Pr(\boldsymbol{V} \le \boldsymbol{V}^{(0)} + \Delta\boldsymbol{V}^{\mathrm{r}} + \Delta\boldsymbol{V}^{\mathrm{p/q}} \\ \qquad -\boldsymbol{S}^{\mathrm{DG}}_{\mathrm{V-P}}\boldsymbol{\omega}_{\mathrm{DG}} \le \overline{\boldsymbol{V}}) \ge 1-\mu_{\mathrm{V}} \\ \inf\limits_{\boldsymbol{\omega}_{\mathrm{DG}}\in U_{\mathrm{DG}}} \Pr(\boldsymbol{V} \le \{\boldsymbol{V}^{(0)} + \Delta\boldsymbol{V}^{\mathrm{r}} + \Delta\boldsymbol{V}^{\mathrm{p}} + \Delta\boldsymbol{V}^{\mathrm{q}} \\ \qquad -S_{\mathrm{V-V}}\Delta V^*_{\mathrm{PCC}} - \boldsymbol{S}^{\mathrm{DG}}_{\mathrm{V-P}}\boldsymbol{\omega}_{\mathrm{DG}}\} \le \overline{\boldsymbol{V}}) \ge 1-\mu_{\mathrm{V}} \end{cases} \tag{29}$$

where μ_V is the DSO's risk tolerance level for the voltage insecurity, satisfying $\mu_V \ge \gamma_1/\gamma_2$; $\boldsymbol{S}^{\mathrm{DG}}_{\mathrm{V-P}}$, $\boldsymbol{S}^{\mathrm{DG}}_{\mathrm{P-P}}$ are the portion of $\boldsymbol{S}_{\mathrm{V-P}}$ and $\boldsymbol{S}_{\mathrm{P-P}}$ about DGs, respectively.

To maximize the P-Q reserve ability, only the transmission capacity constraint at the TSO-DSO interface needs to be satisfied when the DSO provides the P-Q power support. Therefore, the generalized robust chance constraints for the TSO-DSO interface security are formulated by (30).

$$\begin{aligned} \inf_{\boldsymbol{\omega}_{\mathrm{DG}}\in U_{\mathrm{DG}}} \Pr((&P^{(0)}_{\mathrm{PCC}} + \Delta P^{\mathrm{r}}_{\mathrm{PCC}} + \Delta P^{\mathrm{p/q}}_{\mathrm{PCC}} \\ &- (\boldsymbol{S}^{\mathrm{DG}}_{\mathrm{P-P}})^{\mathrm{T}}\boldsymbol{\omega}_{\mathrm{DG}})^2 + (Q^{(0)}_{\mathrm{PCC}} + \Delta Q^{\mathrm{r}}_{\mathrm{PCC}} \\ &+ \Delta Q^{\mathrm{p/q}}_{\mathrm{PCC}})^2 \le S^2_{\mathrm{PCC}}) \ge 1-\mu_{\mathrm{PCC}} \\ \inf_{\boldsymbol{\omega}_{\mathrm{DG}}\in U_{\mathrm{DG}}} \Pr((&P^{(0)}_{\mathrm{PCC}} + \Delta P^{\mathrm{r}}_{\mathrm{PCC}} + \Delta P^{\mathrm{p}}_{\mathrm{PCC}} + \Delta P^{\mathrm{q}}_{\mathrm{PCC}} \\ &- (\boldsymbol{S}^{\mathrm{DG}}_{\mathrm{P-P}})^{\mathrm{T}}\boldsymbol{\omega}_{\mathrm{DG}})^2 + (Q^{(0)}_{\mathrm{PCC}} + \Delta Q^{\mathrm{r}}_{\mathrm{PCC}} \\ &+ \Delta Q^{\mathrm{p}}_{\mathrm{PCC}} + \Delta Q^{\mathrm{q}}_{\mathrm{PCC}})^2 \le S^2_{\mathrm{PCC}}) \ge 1-\mu_{\mathrm{PCC}} \end{aligned} \tag{30}$$

where μ_{PCC} are the DSO's risk tolerance levels for the TSO-DSO interface insecurity, satisfying $\mu_{\mathrm{PCC}} \ge \gamma_1/\gamma_2$.

Two reformulation methods are considered in this paper to reduce the complexity of generalized robust chance constraints.

1) Chebyshev Inequality-based Reformulation Method: the two-sided chance constraints (29) and (30) are first approximately decomposed into single-sided constraints, which are then reformulated to linear counterparts (31) and (32) respectively, based on the Chebyshev inequality [17], [34].

$$\begin{cases} \underline{\boldsymbol{V}} + \hat{\boldsymbol{\theta}}_{\mathrm{V}} + \gamma_{\mathrm{V}}\sqrt{\hat{\boldsymbol{\Sigma}}_{\mathrm{V}}} \le \{\boldsymbol{V}^{(0)} + \Delta\boldsymbol{V}^{\mathrm{r}} + \boldsymbol{S}_{\mathrm{V-V}}\Delta V^*_{\mathrm{PCC}}\} \\ \qquad \le \overline{\boldsymbol{V}} + \hat{\boldsymbol{\theta}}_{\mathrm{V}} - \gamma_{\mathrm{V}}\sqrt{\hat{\boldsymbol{\Sigma}}_{\mathrm{V}}} \\ \underline{\boldsymbol{V}} + \hat{\boldsymbol{\theta}}_{\mathrm{V}} + \gamma_{\mathrm{V}}\sqrt{\hat{\boldsymbol{\Sigma}}_{\mathrm{V}}} \le \boldsymbol{V}^{(0)} + \Delta\boldsymbol{V}^{\mathrm{r}} + \Delta\boldsymbol{V}^{\mathrm{p/q}} \\ \qquad \le \overline{\boldsymbol{V}} + \hat{\boldsymbol{\theta}}_{\mathrm{V}} - \gamma_{\mathrm{V}}\sqrt{\hat{\boldsymbol{\Sigma}}_{\mathrm{V}}} \\ \underline{\boldsymbol{V}} + \hat{\boldsymbol{\theta}}_{\mathrm{V}} + \gamma_{\mathrm{V}}\sqrt{\hat{\boldsymbol{\Sigma}}_{\mathrm{V}}} \le \{\boldsymbol{V}^{(0)} + \Delta\boldsymbol{V}^{\mathrm{r}} + \Delta\boldsymbol{V}^{\mathrm{p}} + \Delta\boldsymbol{V}^{\mathrm{q}} \\ \qquad -\boldsymbol{S}_{\mathrm{V-V}}\Delta V^*_{\mathrm{PCC}}\} \le \overline{\boldsymbol{V}} + \hat{\boldsymbol{\theta}}_{\mathrm{V}} - \gamma_{\mathrm{V}}\sqrt{\hat{\boldsymbol{\Sigma}}_{\mathrm{V}}} \end{cases} \tag{31}$$

where

$$\begin{aligned} \hat{\boldsymbol{\theta}}_V &= \boldsymbol{S}^{\mathrm{DG}}_{\mathrm{V-P}}\boldsymbol{\theta}_{\mathrm{DG}}; \\ \gamma_V &= \sqrt{\gamma_1} + \sqrt{(\gamma_2-\gamma_1)(1-\mu_V)/\mu_V} \\ \hat{\boldsymbol{\Sigma}}_V &= \mathrm{diag}(\boldsymbol{S}^{\mathrm{DG}}_{\mathrm{V-P}}\boldsymbol{\Sigma}_{\mathrm{DG}}(\boldsymbol{S}^{\mathrm{DG}}_{\mathrm{V-P}})^{\mathrm{T}}). \end{aligned}$$

The quadratic parts of (30) are first linearized by regular octagon inner-approximation and then reformulated as (32).

$$\begin{cases} \boldsymbol{a}_{\mathrm{oct}}(P^{(0)}_{\mathrm{PCC}} + \Delta P^{\mathrm{r}}_{\mathrm{PCC}} + \Delta P^{\mathrm{p/q}}_{\mathrm{PCC}}) + \boldsymbol{b}_{\mathrm{oct}}(Q^{(0)}_{\mathrm{PCC}} + \Delta Q^{\mathrm{r}}_{\mathrm{PCC}} \\ \qquad +\Delta Q^{\mathrm{p/q}}_{\mathrm{PCC}}) \le \boldsymbol{c}_{\mathrm{oct}}S_l + \Lambda_l \\ \boldsymbol{a}_{\mathrm{oct}}(P^{(0)}_{\mathrm{PCC}} + \Delta P^{\mathrm{r}}_{\mathrm{PCC}} + \Delta P^{\mathrm{p}}_{\mathrm{PCC}} + \Delta P^{\mathrm{q}}_{\mathrm{PCC}}) \\ \qquad +\boldsymbol{b}_{\mathrm{oct}}(Q^{(0)}_{\mathrm{PCC}} + \Delta Q^{\mathrm{r}}_{\mathrm{PCC}} + \Delta Q^{\mathrm{p}}_{\mathrm{PCC}} + \Delta Q^{\mathrm{q}}_{\mathrm{PCC}}) \\ \qquad \le \boldsymbol{c}_{\mathrm{oct}}S_l + \Lambda_l \\ \Lambda_l = \hat{\theta}_{\mathrm{PCC}}\boldsymbol{a}_{\mathrm{oct}} - \gamma_{\mathrm{PCC}}\sqrt{\mathrm{diag}(\boldsymbol{a}_{\mathrm{oct}}\boldsymbol{a}^{\mathrm{T}}_{\mathrm{oct}})\hat{\Sigma}_{\mathrm{PCC}}} \end{cases} \tag{32}$$

where $\hat{\theta}_{\mathrm{PCC}} = \boldsymbol{\theta}^{\mathrm{T}}_{\mathrm{DG}}\boldsymbol{S}^{\mathrm{DG}}_{\mathrm{P-P}}$; $\hat{\Sigma}_{\mathrm{PCC}} = (\boldsymbol{S}^{\mathrm{DG}}_{\mathrm{P-P}})^{\mathrm{T}}\boldsymbol{\Sigma}_{\mathrm{DG}}\boldsymbol{S}^{\mathrm{DG}}_{\mathrm{P-P}}$; $\gamma_{\mathrm{PCC}} = \sqrt{\gamma_1} + \sqrt{(\gamma_2-\gamma_1)(1-\mu_{\mathrm{PCC}})/\mu_{\mathrm{PCC}}}$.

The reformulation is easy to be implemented. However, the reformulation accuracy is sensitive to the risk tolerance level. It has been verified in [23], [35] that the robustness under this reformulation can be ensured by appropriately choosing the risk tolerance level.

2) Duality theory-based reformulation method: to enhance the robustness for large risk tolerance levels, a duality theory-based reformulation method is proposed in [36]. In this paper, this method is extended to be suitable for generalized robust chance constraints under the generalized ambiguity set. Using the first constraint in (29) as an example, it can be reformulated to (33) for each bus i. The proof is shown in Appendix B.

$$\begin{cases} y_i^2 + (\gamma_2 - \gamma_1\delta_i^2)\hat{\Sigma}_{\mathrm{V},i} \le \mu_{\mathrm{V}}(\underline{V}_i + S^{\mathrm{DG}}_{\mathrm{V-P},i}\boldsymbol{\theta}_{\mathrm{DG}} - \pi_i)^2 \\ \underline{V}_i + S^{\mathrm{DG}}_{\mathrm{V-P},i}\boldsymbol{\theta}_{\mathrm{DG}} \le \pi_i \le \overline{V}_i + S^{\mathrm{DG}}_{\mathrm{V-P},i}\boldsymbol{\theta}_{\mathrm{DG}} \\ |V_i^{(0)} + \Delta V_i^{\mathrm{r}} + S_{\mathrm{V-V},i}\Delta V^*_{\mathrm{PCC}}| \le y_i - \sqrt{\gamma_1}\sqrt{\hat{\Sigma}_{\mathrm{V},i}}\delta_i + \pi_i \\ y_i \ge 0,\ \delta_i \ge 0 \end{cases} \tag{33}$$

where y_i, π_i and δ_i are auxiliary variables; $\hat{\boldsymbol{\Sigma}}_{V,i}$, $\boldsymbol{S}^{\mathrm{DG}}_{\mathrm{V-P},i}$ and $\boldsymbol{S}_{\mathrm{V-V},i}$ are the i-th element of $\hat{\boldsymbol{\Sigma}}_V$, the i-th row of $\boldsymbol{S}^{\mathrm{DG}}_{\mathrm{V-P}}$, and the i-th element of $\boldsymbol{S}_{\mathrm{V-V}}$ respectively.

Each constraint in (29)–(30) can be reformulated by the same method as (33), which is not exhibited due to the space limit.

The reformulation model (33) is a generalized form, which can be equal to the model in [36] by setting $\gamma_1 = 0$, $\gamma_2 = 1$. Compared to the first reformulation method, this method will bring in second-ordered convex constraints and extra variables.

As a result, the multi-objective optimization model integrating GRCC and CSMC (GRCC-CSMC) for V-PQRC evaluation is formulated by the combination of objectives and constraints, as shown in (34).

$$\begin{aligned} &\max \boldsymbol{F}(\boldsymbol{x}) = [F_1(\boldsymbol{x}), F_2(\boldsymbol{x}), F_3(\boldsymbol{x})]^{\mathrm{T}} \\ &\text{s.t.}\ \ \boldsymbol{\Phi} : \pi \begin{cases} \text{(17)–(23), (25)–(28)} \\ \text{(31)–(32) or (33) form} \end{cases} \end{aligned} \tag{34}$$

It is a multi-objective convex programming problem which can be solved by the nondominated sorting genetic algorithm II (NSGA-II). Instead of converting this problem into a single-objective problem, the NSGA-II can find multiple Pareto optimal solutions in one single simulation run [37]. As a result, the diversity of Pareto optimal solutions can be ensured with a smaller computational burden. The detailed procedure of the NSGA-II algorithm is shown in Appendix C.

After optimization, the objective vector $\boldsymbol{F}$ corresponding to Pareto optimal solution set $\boldsymbol{S}_{\mathrm{r}}$ refers to the Pareto optimal P-Q reserve schemes that cannot be dominated by any other feasible scheme. Therefore, the Pareto front surface constructed by $\boldsymbol{F}$ can be recognized as the boundary of V-PQRC.

V. Non-Approximated Selecting Method for the V-PQRC Linear Model

Since the Pareto front surface is too nonlinear to be directly modeled, the piecewise linearization method is an alternative approach to build up a linear model of V-PQRC based on the Pareto optimal reserve schemes. The V-PQRC linear model can be expressed as a set of linear inequalities. On the perspective of the space geometric, the model is regarded as a closed space bounded by a polyhedron with all the Pareto optimal reserve schemes as vertices. However, the massive amount of the reserve schemes results in a high model complexity. The non-approximated selecting (NAS) method is proposed in this paper to preserve a small batch of Pareto optimal reserve schemes to build up the V-PQRC linear model so that the model complexity can be reduced.

The normalization Euclidean distance (*NED*) formulated by (35) is used to judge whether the Pareto optimal reserve scheme i, ($\boldsymbol{F}_i = [P_{\mathrm{res}}(i), Q_{\mathrm{res}}(i), \Delta V^*_{\mathrm{PCC}}(i)]^{\mathrm{T}}$) can replace scheme j.

$$\begin{aligned} &\textit{NED}_{ij} = \\ &\sqrt{\left(\frac{P_{\mathrm{res}}(i) - P_{\mathrm{res}}(j)}{\overline{P}_{\mathrm{res}} - \underline{P}_{\mathrm{res}}}\right)^2 + \left(\frac{Q_{\mathrm{res}}(i) - Q_{\mathrm{res}}(j)}{\overline{Q}_{\mathrm{res}} - \underline{Q}_{\mathrm{res}}}\right)^2 + \left(\frac{\Delta V^*_{\mathrm{PCC}}(i) - \Delta V^*_{\mathrm{PCC}}(j)}{\Delta\overline{V}^*_{\mathrm{PCC}} - \Delta\underline{V}^*_{\mathrm{PCC}}}\right)^2} \end{aligned} \tag{35}$$

where $\overline{P}_{\mathrm{res}}$ and $\underline{P}_{\mathrm{res}}$ are the maximal upward and downward P reserves of Pareto optimal reserve schemes, respectively; $\overline{Q}_{\mathrm{res}}$ and $\underline{Q}_{\mathrm{res}}$ are the maximal inductive and capacitive Q reserves, respectively; $\Delta\overline{V}^*_{\mathrm{PCC}}$ and $\Delta\underline{V}^*_{\mathrm{PCC}}$ are the maximal and minimal voltage deviation limits at the TSO-DSO interface, respectively.

The scheme i can replace scheme j, when $\textit{NED}_{ij}$ is smaller than the permitted approximation range ($\overline{\textit{NED}}$).

The NAS method aims to preserve the non-approximated Pareto optimal reserve schemes. When all non-approximated solutions are preserved, the reserve scheme set $\boldsymbol{F}$ can be equivalently replaced by them. Then, the V-PQRC linear model formulated by the much smaller batch can reduce the model complexity and satisfy the permitted approximate error range.

The detailed procedure is listed in Algorithm 1. First, the first-level non-approximated reserve scheme set $\boldsymbol{F}_n$ is selected from $\boldsymbol{F}$. $\boldsymbol{F}_n$ contains the key non-approximated Pareto optimal reserve schemes containing the maximum values of the TSO-

Algorithm 1: Non-approximated selecting (NAS) method

Input: Pareto optimal reserve scheme set S_{r}; range $\overline{\textit{NED}}$;

Step 1: Generate the first-level non-approximated scheme set $\boldsymbol{F}_n$ $\boldsymbol{F}_n = \{F|_{\Delta\overline{V}^*_{\mathrm{PCC}}}, F|_{\Delta\underline{V}^*_{\mathrm{PCC}}}, F|_{\overline{P}_{\mathrm{res}}}, F|_{\underline{P}_{\mathrm{res}}}, F|_{\overline{Q}_{\mathrm{res}}}, F|_{\underline{Q}_{\mathrm{res}}}\}$;

for $i = 1$ *to length*($\boldsymbol{F}_n$) -1 **do**

  calculate $\textit{NED}_{ij}$ by (33), $\forall j \in \{\boldsymbol{F}_n \backslash \boldsymbol{F}_n(i)\}$;

  if $\textit{NED}_{ij} \le \overline{\textit{NED}}$ **then**

    remove the approximated solution, $\boldsymbol{F}_n \leftarrow \{\boldsymbol{F}_n \backslash \boldsymbol{F}_n(j)\}$;

  end

end

Step 2: Generate the second-level non-approximated scheme set $\boldsymbol{F}'_n$

Initialize $\boldsymbol{F}'_n$: $\boldsymbol{F}'_n = \{F|F$ is non-approximated by $\boldsymbol{F}_n\}$;

for $i = 1$ *to length*($\boldsymbol{F}'_n$) -1 **do**

  calculate $\textit{NED}_{ij}$ by (33), $\forall j \in \{\boldsymbol{F}'_n \backslash \boldsymbol{F}'_n(i)\}$;

  if $\textit{NED}_{ij} \le \overline{\textit{NED}}$ **then**

    remove the approximated solution, $\boldsymbol{F}'_n \leftarrow \{\boldsymbol{F}'_n \backslash \boldsymbol{F}'_n(j)\}$;

  end

end

Output: non-approximated solution set $\boldsymbol{F}_l \leftarrow \boldsymbol{F}_n \cup \boldsymbol{F}'_n$

DSO interface voltage deviation limit, P reserve and Q reserve in $\boldsymbol{F}$, so that these characteristics can be preserved in the V-PQRC linear model. Then, the second-level non- approximated reserve scheme set $\boldsymbol{F}_n'$ is selected from the rest of $\boldsymbol{F}$. After two steps, the amount of Pareto optimal reserve schemes can be significantly reduced. By combining $\boldsymbol{F}_n$ and $\boldsymbol{F}_n'$, the non-approximated reserve scheme set $\boldsymbol{F}_l$ is obtained.

Using the NAS method, the V-PQRC can be recognized as a closed space bounded by a polyhedron with the solutions in S_l as vertices. The V-PQRC linear model is formulated by (36).

$$\boldsymbol{\Gamma}_{\mathrm{res}} \Leftrightarrow \boldsymbol{A}_l \begin{bmatrix} P_{\mathrm{res}} \\ Q_{\mathrm{res}} \\ \Delta V_{\mathrm{PCC}}^{*} \end{bmatrix} + \boldsymbol{B}_l \leq 0 \tag{36}$$

where $\boldsymbol{A}_l$ and $\boldsymbol{B}_l$ are the linear parameter matrixes, according to the non-approximated scheme set $\boldsymbol{F}_l$.

VI. Simulation Studies

A. Simulation Settings

The proposed V-PQRC evaluation method is simulated in the modified IEEE 33-bus distribution system, as shown in Fig. 6. The detailed initial operation state is provided in [38]. Bus 1 is defined as the TSO-DSO interface and the initial voltage is set to be 1 p.u. DGs at bus 8, 12, 17, 21, 25, 31, 32 and 33 are available to provide reserves. The installed capacity of each DG is 0.5 MVA. The initial active and reactive output power of each DG are set to be 372 kW and 0 kvar, respectively. The rest buses are integrated with FLs. The downward and upper limits ($\Delta P_{\mathrm{FL},i}^{\mathrm{down}}$ and $\Delta P_{\mathrm{FL},i}^{\mathrm{up}}$) for the FLs at each bus are -20% and 40% of the initial active load. The lower and upper limits for the active exchange power fluctuation ($\Delta\overline{P}_{\mathrm{PCC}}$ and $\Delta\underline{P}_{\mathrm{PCC}}$) are -5 MW and 5 MW. The transmission capacity at TSO-DSO interface is 10 MVA. The dispatch interval is 15 minutes.

The sensitivity matrixes and vectors ($\boldsymbol{S}_{\mathrm{V-P}}$, $\boldsymbol{S}_{\mathrm{V-Q}}$, $\boldsymbol{S}_{\mathrm{V-V}}$, $\boldsymbol{S}_{\mathrm{P-P}}$, $\boldsymbol{S}_{\mathrm{P-Q}}$, $\boldsymbol{S}_{\mathrm{P-V}}$, $\boldsymbol{S}_{\mathrm{Q-P}}$, $\boldsymbol{S}_{\mathrm{Q-Q}}$) in the linearized power flow constraints (14)–(17) are calculated by repeatedly conducting power flow simulation via the MATPOWER toolbox. At each simulation run, randomly perturb the power of DGs and FLs. The average values of each are used in this paper.

1) Uncertainty Settings

DG uncertainty $\boldsymbol{\omega}_{\mathrm{DG}}$: the forecasting errors between the most recent forecasted data and the measured data of the aggregate Belgian wind farms [39], from Jan. 2020 to Mar. 2021, are used as the DG uncertainty dataset and scaled to the $P_{\mathrm{DG},i}^{(0)}$ situation. The forecasting interval is 15 minutes. Their dataset size is 5,000, and 1,000 and are randomly selected as historical data to calculate the estimates ($\boldsymbol{\theta}_{\mathrm{DG}}$ and $\boldsymbol{\Sigma}_{\mathrm{DG}}$) in the generalized ambiguity set (10). γ_1 and γ_2 are set to be 0.1 and 1.1 respectively, to avoid being overly conservative [24].

Although only the wind power uncertainty is utilized in this simulation, the proposed V-PQRC evaluation method can be applicable for other types of DGs.

FL uncertainty $\boldsymbol{\omega}_{\mathrm{FL}}$: the control timestep of the CSMC is set to 0.1 s. The aggregated FL uncertainty at each control timestep is a random variable following a uniform distribution on $[-\overline{\omega}_{\mathrm{FL},i}, \overline{\omega}_{\mathrm{FL},i}]$, where $\overline{\omega}_{\mathrm{FL},i}$ is 15% of $\Delta P_{\mathrm{FL},i}^{\mathrm{up}}$. The CSMC validity constraint (10) is built up based on above.

2) Uncertainty Scenario Set

5,000 uncertainty scenarios are set to test the performance of the V-PQRC evaluation method. In each scenario, the DG uncertainty is chosen from the DG uncertainty dataset above, and the FL uncertainty satisfies the FL uncertainty setting.

If there is no emphasis, the V-PQRC evaluation results are obtained via the GRCC-CSMC multi-objective optimization using the Chebyshev inequality-based reformulation method.

B. V-PQRC Evaluation Results

The risk tolerance levels μ_V and μ_l are both set to be 0.2 in this case. After the V-PQRC evaluation, 960 Pareto optimal reserve schemes are obtained. Then, the V-PQRC linear model is constructed via the NAS method with $\overline{NED} = 0$. As shown in Fig. 7(a), the V-PQRC linear model is a closed polyhedron, and each P-Q reserve scheme inside the space can be realized without offending the distribution system operation security.

1) Necessity of Considering the Voltage Deviation Limit at the TSO-DSO Interface ($\Delta V_{\mathrm{PCC}}^{*}$) in the V-PQRC Evaluation

The 2-D PQRC feasible region with given $\Delta V_{\mathrm{PCC}}^{*}$ is the $\Delta V_{\mathrm{PCC}}^{*}$-axis cross section of the V-PQRC linear model, as shown in Fig. 7(b). According to Fig. 7(b), the PQRC feasible regions will change along with the change of the given $\Delta V_{\mathrm{PCC}}^{*}$.

The voltage security of the maximal capacitive Q reserve scheme with $\Delta V_{\mathrm{PCC}}^{*} = 0$ is investigated under different voltage deviations at the TSO-DSO interface (ΔV_{PCC}), to demonstrate the necessity of considering $\Delta V_{\mathrm{PCC}}^{*}$ in the V-PQRC evaluation. According to the obtained V-PQRC linear

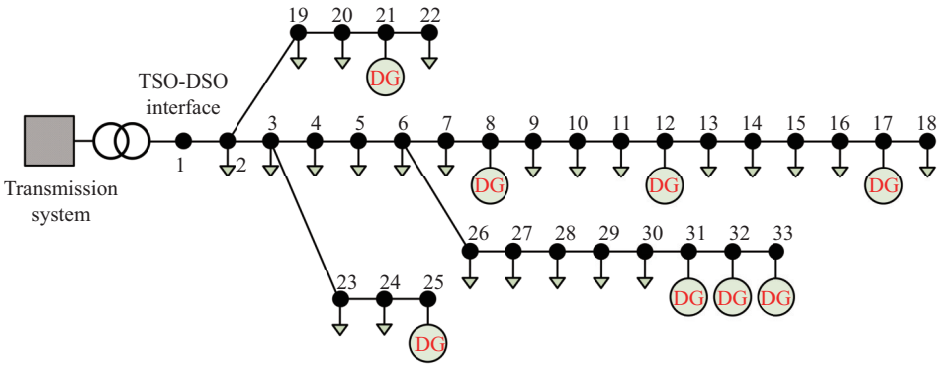

Fig. 6. The modified IEEE 33-bus distribution system.

model, the DSO can provide −4.44 Mvar Q power support to the TSO. The reserve allocation results are shown in Appendix D.

The robust feasibility of voltage security chance constraints (29) is analyzed under two situations: (a) the DSO provides the Q power support; (b) the DSO does not provide the support. The value of ΔV_{PCC} after two situations is set to 0, 0.017 p.u. and −0.017 p.u., respectively. The results are shown in Figs. 8 and 9. According to (31), the upper and lower limits of the chance constraints are $\overline{\boldsymbol{V}} + \hat{\boldsymbol{\theta}}_V - \gamma_V \sqrt{\hat{\boldsymbol{\Sigma}}_V}$ and $\underline{\boldsymbol{V}} + \hat{\boldsymbol{\theta}}_V - \gamma_V \sqrt{\hat{\boldsymbol{\Sigma}}_V}$.

According to Fig. 8, when $\Delta V_{\mathrm{PCC}} = 0$, the bus voltage is within the limits of the voltage chance constraint after the DSO providing the Q power support, so that the reserve scheme is reliable to ensure the voltage security.

However, when ΔV_{PCC} increases to 0.017 p.u. after providing the Q power support, the upper limits at some buses are broken, as shown in Figs. 8 and 9. So that the reserve scheme is not robust when $\Delta V_{\mathrm{PCC}} = 0.017$ p.u., and the overvoltage risk will be higher beyond the tolerance. For the sake of voltage security, the capacitive Q reserve ability should be restricted.

The reserve scheme is also not robust when $\Delta V_{\mathrm{PCC}} = -0.017$ p.u. According to Fig. 9, the voltage of some buses has a significantly intolerable risk to drop below 0.95 p.u. in situation (b). More response power of DGs and FLs should be re-dispatched to raise the voltage at the beginning of dispatch interval, instead of providing reserves, to ensure the voltage security for different power support situations.

Therefore, it is essential to involve $\Delta V^*_{\mathrm{PCC}}$ in the V-PQRC evaluation to ensure the reliability of the P-Q reserve scheme under any possible ΔV_{PCC} within $\Delta V^*_{\mathrm{PCC}}$.

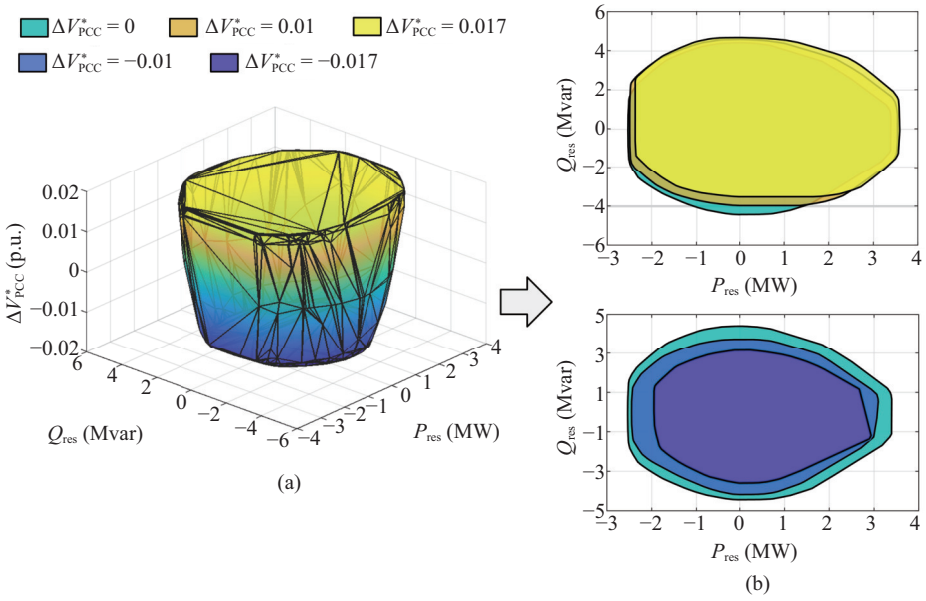

Fig. 7. Illustration of the V-PQRC linear model and its 2-D feasible regions. (a) V-PORC linear model with $\overline{NED} = 0$. (b) 2-D PORC feasible regions under different ΔV_{PCC}.

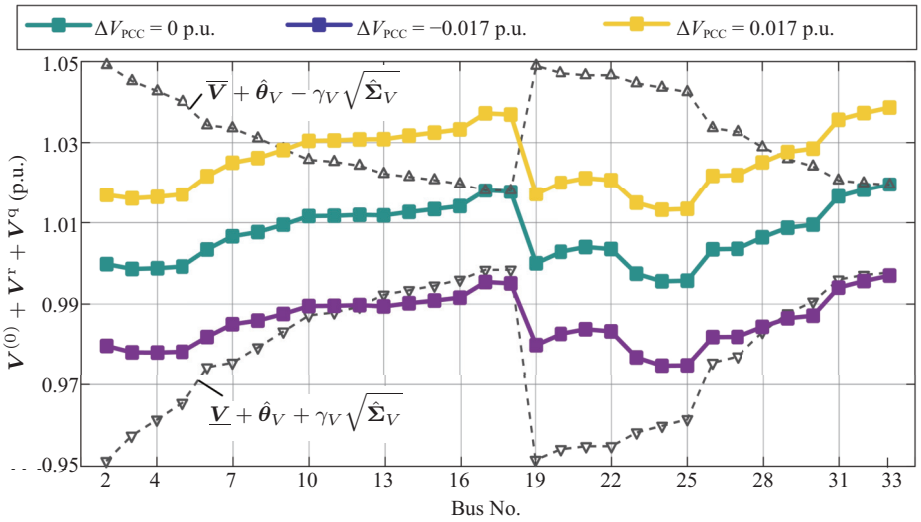

Fig. 8. Robust feasibility results of the voltage security chance constraint under different ΔV_{PCC} in situation (a).

2) Influence of The Risk Tolerance Level

Maximal P_{res}, Q_{res}, and ΔV^*_{PCC} under different risk tolerance levels are listed in Table I. It is demonstrated that the P-Q reserve ability of the DSO can be strengthened with larger risk tolerance levels. Since larger tolerance levels allow higher probabilities to break security constraints, more response capacities of DGs and FLs can be utilized to provide reserves.

The PQRC feasible regions with different given ΔV^*_{PCC} and risk tolerance levels are considered, as illustrated in Fig. 10. It can be found that the Q reserve ability is more sensitive to the change of the risk tolerance level than P reserve ability. This is because the high R/X ratios (>1) in the testing system make the bus voltage less sensitive to the reactive power injection.

TABLE I
MAXIMAL P_{res}, Q_{res}, AND ΔV^*_{PCC} UNDER DIFFERENT RISK TOLERANCE LEVELS

Risk tolerance level ($\mu_V = \mu_l$)		0.2	0.3	0.4	0.5
P_{res} (MW)	downward	−2.491	−2.562	−2.610	−2.611
	upward	3.591	3.660	3.703	3.717
Q_{res} (Mvar)	capacitive	−4.442	−5.153	−5.575	−5.803
	inductive	4.633	5.309	5.763	6.059
ΔV^*_{PCC} (p.u.)	drop	−0.017	−0.031	−0.039	−0.040
	rise	0.017	0.032	0.041	0.048
CPU time (s)		44.21	43.43	44.44	44.13

When the voltage security constraints are relaxed, the feasible range for the reactive power injection at each bus is more obviously expanded to enhance the Q reserve ability. As listed in Table I, the maximal Q reserve capacities increase about

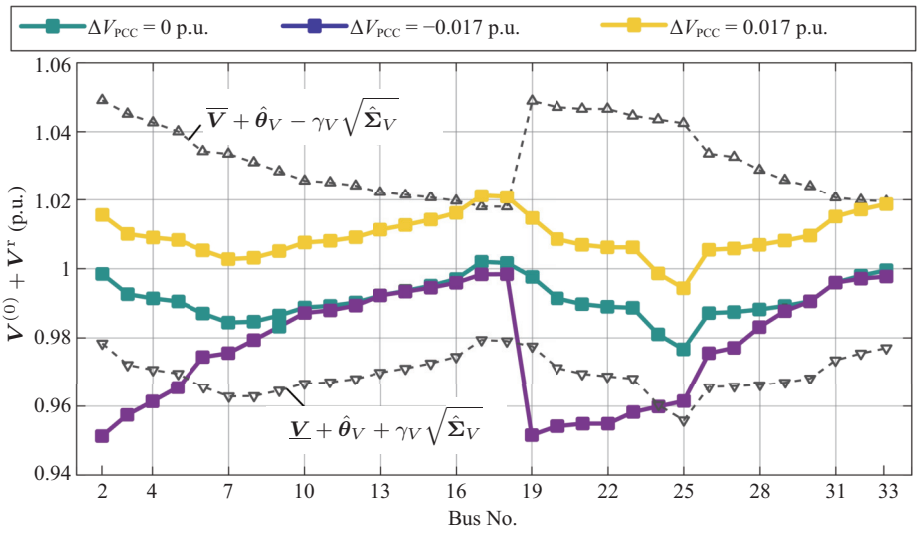

Fig. 9. Robust feasibility results of the voltage security chance constraint under different ΔV_{PCC} in situation (b).

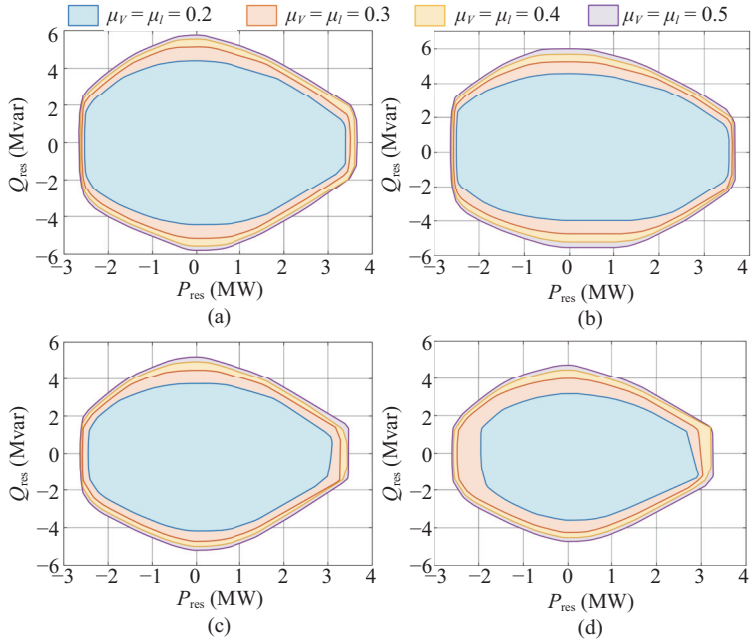

Fig. 10. The PQRC feasible regions with different given ΔV^*_{PCC} and μ_V. (a) $\Delta V^*_{\text{PCC}} = 0$ p.u. (b) $\Delta V^*_{\text{PCC}} = 0.01$ p.u. (c) $\Delta V^*_{\text{PCC}} = -0.01$ p.u. (d) $\Delta V^*_{\text{PCC}} = -0.017$ p.u.

30% when the risk tolerance level rises from 0.2 to 0.5, while the maximal P reserve capacities only increase 4%.

Therefore, the DSO should decide a proper risk tolerance level to provide desired reserves, and equip extra voltage regulation resources if necessary to compensate the risk.

C. Robustness of the V-PQRC evaluation

To verify the robust performance of the V-PQRC evaluation, the obtained Pareto optimal reserve schemes are tested on the 5,000 uncertainty scenarios. The FL response time in each scenario is randomly chosen from 1 s to 3 s. Considering the FL uncertainty fluctuates over the whole dispatch interval, the final FL response power is of concern. Power flow is conducted to obtain actual P reserve and Q reserve results for each reserve scheme in each uncertainty scenario.

The evaluation error and mean insecurity probability are investigated in this case to reveal the robust performance. The P and Q reserve evaluation errors, i.e., $\sigma_{\rm res}^{\rm P}$ and $\sigma_{\rm res}^{\rm Q}$, are the root mean squared errors of P and Q reserve evaluation results, respectively. The mean insecurity probability is defined as the mean probability of the Pareto optimal reserve schemes to violate the voltage security or TSO-DSO interface security constraints.

Use the single GRCC method-based evaluation method as the comparison, which captures the uncertainties of DGs and FLs by one generalized ambiguity set, without using the CSMC. The test results are listed in Tables II and III.

TABLE II
ACTIVE AND REACTIVE POWER RESERVE EVALUATION ERRORS

Risk tolerance level	$\sigma_{\rm res}^{\rm P}$ (MW)		$\sigma_{\rm res}^{\rm Q}$ (Mvar)	
	GRCC	GRCC-CSMC	GRCC	GRCC-CSMC
0.2	1.121	0.873	0.465	0.426
0.3	1.124	0.872	0.504	0.438
0.4	1.122	0.874	0.658	0.516
0.5	1.121	0.873	0.886	0.537

TABLE III
MEAN INSECURITY PROBABILITY TESTING RESULTS

Risk tolerance level	Single GRCC	GRCC-CSMC
0.2	25.62%	18.17%
0.3	31.57%	24.28%
0.4	32.75%	28.64%
0.5	37.25%	31.81%

It is verified that by integrating GRCC and CSMC in the proposed V-PQRC evaluation method, the evaluation errors and mean insecurity probability are obviously reduced. This is because the proposed CSMC can smooth the FL uncertainty during response so that the system security operation won't be disturbed by it. However, the single GRCC method can only consider the FL uncertainty in evaluation but cannot really smooth it. Furthermore, CSMC only needs the boundary information of the FL uncertainty, which is easy to obtain.

Thereby, the V-PQRC evaluation based on the GRCC-CSMC method is easy to be implemented, and more robust under the uncertainties of DGs and FLs.

1) Performances under different ambiguity sets: Three different ambiguity sets are compared in this case:

A1: The generalized ambiguity set (10) used in this paper;

A2: The ambiguity set in [23] assuming that the actual mean and covariance matrix are equal to the estimated values;

A3: The Wasserstein metric-based ambiguity set in [20] and the confidence level is set to 0.95.

The Chebyshev inequality-based reformulation is utilized for chance constraints under A1 and A2. The chance constraints under A3 are reformulated into the linear formulations in [20]. We compare the conservative and robust performances of V-PQRC evaluation under above ambiguity sets when the risk tolerance level is set to 0.5. The results are listed in Table IV.

TABLE IV
MAXIMAL $P_{\rm res}$, $Q_{\rm res}$, AND $\Delta V_{\rm PCC}^{*}$, MEAN INSECURITY PROBABILITY TESTING RESULTS UNDER DIFFERENT AMBIGUITY SETS

Ambiguity set		A1	A2	A3
$P_{\rm RES}$ (MW)	downward	−2.611	−2.707	−2.670
	upward	3.717	3.735	3.722
$Q_{\rm RES}$ (Mvar)	capacitive	−5.803	−6.046	−5.988
	inductive	6.059	6.485	6.380
$\Delta V_{\rm PCC}^{*}$ (p.u.)	drop	−0.040	−0.042	−0.042
	rise	0.048	0.052	0.049
Mean insecurity probability		31.81%	51.85%	45.37%

According to Table IV, the V-PQRC evaluation under A1 is more conservative than the other ambiguity sets. The mean insecurity probability under A1 is smallest, which reveals that the reserve evaluation under A1 is most robust. Although the utilization of A2 shows the least conservativeness, the evaluation is not robust because of the inadequate historical data results in large estimation errors of the mean and the covariance matrix. The utilization of A3 is slightly less conservative than A1, but the robust performance is obviously less than A1 and the modeling of A3 is more complex. Thus, the generalized ambiguity set is more suitable in this paper to ensure the robustness of the V-PQRC evaluation with inadequate historical data.

It must be emphasized that A2 and A3 can show better performances with more historical data. Thus, the ambiguity set should be chosen based on the features of historical data. And the proposed V-PQRC evaluation method can still be valid.

2) Performances under different reformulation methods: The conservative and robust performances of the V-PQRC evaluation via the duality theory-based reformulation are listed in Table V.

TABLE V
PERFORMANCES UNDER THE DUALITY THEORY-BASED REFORMULATION

Risk tolerance level ($\mu_V = \mu_l$)		0.2	0.3	0.4	0.5
$P_{\rm RES}$ (MW)	downward	−2.497	−2.579	−2.625	−2.655
	upward	3.323	3.598	3.646	3.677
$Q_{\rm RES}$ (Mvar)	capacitive	−3.974	−4.929	−5.438	−5.708
	inductive	4.094	5.123	5.620	5.925
$\Delta V_{\rm PCC}^{*}$ (p.u.)	drop	−0.009	−0.026	−0.036	−0.039
	rise	0.009	0.026	0.036	0.039
Mean insecurity probability		17.58%	23.41%	26.70%	29.13%
CPU time (s)		43.63	44.30	44.91	45.18

Results in Table V with Tables I and II confirm that the duality theory-based reformulation is less relaxed than the

Chebyshev inequality-based method. The V-PQRC evaluation is more conservative under each risk tolerance level, to reduce the mean insecurity probability. It reveals that the robust performance of this method is better, and the advantage becomes more obvious along with the increase of the risk tolerance level. Although new variables are added by this method, the CPU time is similar to the other method. It implies that the computational burden of the V-PQRC evaluation will not be increased when using this method for chance constraints.

According to the comprehensive results, it can be concluded that the Chebyshev inequality-based reformulation method does well to achieve a balance between conservativeness and robustness when the risk tolerance level is small. The duality theory-based method is more suitable under lager risk tolerance levels to ensure a good robust performance. The DSO should select from them according to risk tolerance level setting.

D. Simplification Performances of The NAS Method

The Pareto optimal reserve schemes under $\mu_V = \mu_l = 0.2$ are utilized to formulate the V-PQRC linear model by the NAS method. The V-PQRC model complexity under different is listed in Table VI. The number of preserved schemes and the model dimension are two concerned indexes. The model dimension is the number of inequalities in the V-PQRC linear model.

TABLE VI
MODEL COMPLEXITY UNDER DIFFERENT PERMITTED APPROXIMATION ERRORS

$\overline{NED}$	Number of preserved schemes	Model dimension
0	960	1102
0.2	137	224
0.4	78	134
0.6	49	88
0.8	37	70

It can be observed from Table VI that the number of preserved schemes and the model dimension are significantly reduced with a larger $\overline{NED}$. When $\overline{NED}$ is set to be 0, all the Pareto optimal reserve schemes are preserved and the model dimension is up to 1,102, which is too high to act as a constraint in the transmission system operation optimization. When $\overline{NED}$ is set to be 0.8, only 4% Pareto optimal reserve schemes are preserved to build the V-PQRC linear model and the model dimension can be reduced by nearly 94%.

The influences of the NAS method on V-PQRC model robustness and accuracy are discussed further. The PQRC feasible regions with different $\overline{NED}$ are illustrated in Fig. 11, where red points represent the Pareto optimal reserve schemes.

As shown in Fig. 11, under each given $\Delta V^*_{\mathrm{PCC}}$, the PQRC feasible region under a larger $\overline{NED}$ is the subset of the primary feasible region under $\overline{NED} = 0$. That means the robustness of the V-PQRC evaluation is still valid when using the NAS method.

Furthermore, the PQRC feasible region under $\overline{NED} = 0.2$ is almost the same as the region under $\overline{NED} = 0$, but the model demission is reduced by about 80%. The simplification is achieved by sacrificing the feasible space, so that the model accuracy is reduced, because some Pareto optimal reserve schemes are mistakenly treated as infeasible schemes.

To quantify the V-PQRC model accuracy, the deviation of each Pareto optimal reserve scheme from the V-PQRC model with given $\Delta V^*_{\mathrm{PCC}}$ is calculated. The deviation of Pareto optimal reserve schemes inside the V-PQRC model is set to 0. Then, the mean deviation is utilized as the index for model accuracy, and the results are listed in Table VII.

According to Table VII, the model accuracy will not be heavily reduced by the NAS method when choosing a proper $\overline{NED}$. In this case, $\overline{NED} = 0.6$ is appropriate, which can reduce

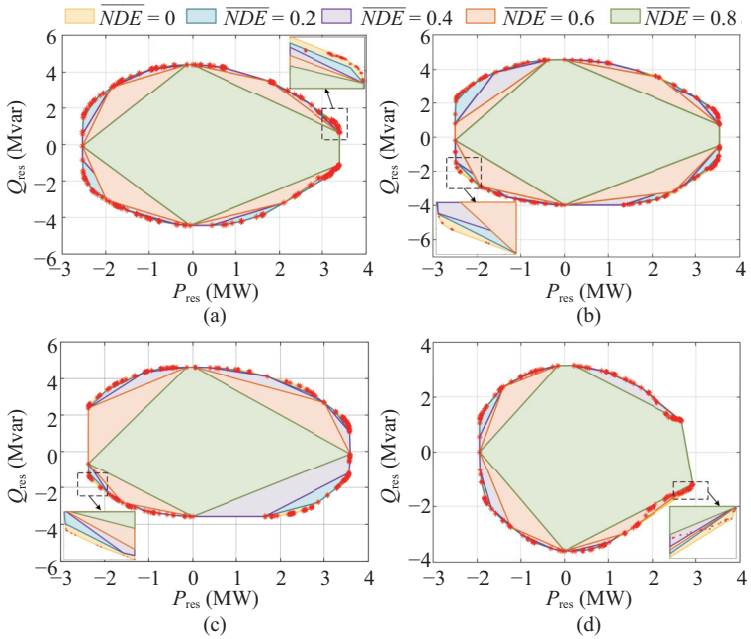

Fig. 11. Illustration of 2-D PQRC feasible regions under different $\overline{NED}$. (a) $\Delta V^*_{\mathrm{PCC}} = 0$ p.u. (b) $\Delta V^*_{\mathrm{PCC}} = 0.01$ p.u. (c) $\Delta V^*_{\mathrm{PCC}} = -0.01$ p.u. (d) $\Delta V^*_{\mathrm{PCC}} = -0.017$ p.u.

TABLE VII
MODEL ACCURACY UNDER DIFFERENT PERMITTED APPROXIMATION ERRORS

$\overline{NED}$	Mean deviation of Pareto optimal schemes from V-PQRC model
0	0 MVA
0.2	0.03 MVA
0.4	0.11 MVA
0.6	0.27 MVA
0.8	0.63 MVA

TABLE VIII
T-D SYSTEM COORDINATED OPERATION CASE SETTINGS

Case	Case 1	Case 2
Reserve request	$\langle 1$ MW, 4 Mvar, 0.01 p.u.$\rangle$	$\langle -1$ MW, -4 Mvar, -0.01 p.u.$\rangle$
Disturbance	the load at bus 97 reduces 5 MW and 50 Mvar demand	the load at bus 97 increases 5 MW and 50 Mvar demand
Target	$\Delta V_{97} \leq 0.01$ p.u.	$\Delta V_{97} \geq -0.01$ p.u.

the model dimension from 1,606 to 104, while preserving a relatively large subset of the primary V-PQRC feasible space.

E. Simple Application in T-D System Coordinated Operation

The T-D system illustrated in Fig. 2 is used in this case study. According to the V-PQRC evaluation results above, the reserve potential of a single modified IEEE-33 distribution system is very limited for the transmission system. In order to more obviously show the effect of V-PQRC evaluation in the T-D system coordinated operation, five distribution systems are connected to bus 97 of the IEEE-118 bus transmission system. Each of them is the same as the modified IEEE-33 bus system shown in Fig. 6. The total power supports of five distribution systems are investigated in the case study.

The T-D system is modeled and simulated by the MATPOWER toolbox. To clearly observe the effectiveness of the T-D system coordinated operation, it is assumed that the voltage loss between bus 97 and the TSO-DSO interface bus (i.e., transformer voltage loss) can be ignored, and the voltage at the TSO-DSO interface of each distribution system is the same as the voltage at bus 97. A load with 11 MW and 19 Mvar demand is also connected to bus 97, so that the initial voltage at each TSO-DSO interface bus can be maintained to 1 p.u.. Thus, the V-PQRC evaluation results of each distribution system are equal to the results listed above. The V-PQRC linear model under $\overline{NED} = 0.6$ in Part D is chosen as the V-PQRC model for each distribution system. The DG an FL uncertainties are randomly chosen from the uncertainty scenario set.

Two cases listed in Table VIII are simulated. In each case, the TSO sends the reserve request to each DSO for the five distribution systems at the beginning of the dispatch interval, and the disturbance occurs in the interval. The TSO should coordinate the reserve resources in the transmission system and the support from DSOs to drive the voltage deviation at bus 97 (ΔV_{97}) to reach the target.

In each case, each DSO re-dispatches and allocates the reserve requests among DGs and FLs according to the reserve request. The results in each distribution system are shown in Figs. 12 and 13. It can be found that the DGs use the main role to provide P and Q reserves, and the DGs closer to the TSO-DSO interface (e.g., bus 8, 12, 21 and 25) contributes more. The FLs also participate in the reserve provision, but their main responsibility is to avoid the bus voltage out of limits after the DSO provides power supports, because FLs are distributed more widely and high R/X ratios make them nice resources to improve the voltage security.

Suppose that bus 96 in the transmission system equips enough reserves for the TSO's target, the comparison of the power supports from bus 96 and the distribution systems is listed in Table IX. All results are obtained from the T-D system simulation via the MATPOWER toolbox.

When using the reserve of the distribution systems, the DSOs are required to provide all the P-Q reserve capacities to support the transmission system voltage regulation. The control command of DSOs for DGs and FLs to provide support are the same as the reserve allocation shown in Figs. 12 and 13. However, due to the DG and FL uncertainties, the provided P-Q power may differ from the desired values. The TSO controls

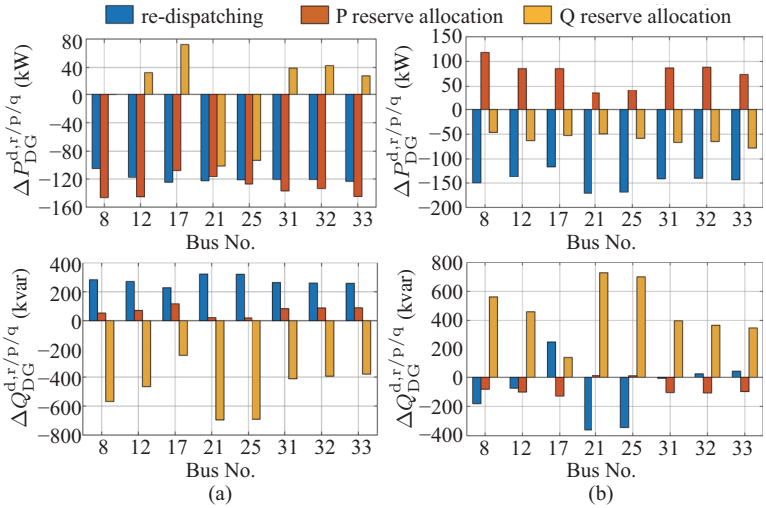

Fig. 12. The re-dispatching and reserve allocation results of DGs in each case. (a) Case 1. (b) Case 2.

resources are in bus 96 to assist DSOs to drive ΔV_{97} to reach the targeted value. Since the power support from each distribution system is the same, only their total power support is listed in Table IX.

However, if no support is provided, ΔV_{97} will reach to 0.027 p.u. in Case 1 and drop to -0.027 p.u. in Case 2. To drive ΔV_{97} to reach the targets, the neighboring bus 96 needs to solely provide 110 Mvar inductive reactive power support in Case 1, and 110 Mvar capacitive reactive power support in Case 2. However, when utilizing the distribution systems as localized virtual reserve resources, DSOs can totally provide 20.9 Mvar inductive reactive power support in Case 1 and 19.45 Mvar capacitive reactive power support in Case 2, so that the supports from bus 96 are obviously reduced. Therefore, the reserve resources in the transmission system can be significantly saved by exploiting the reserve potential of the distribution systems.

The bus voltage inside each distribution system after providing the power support is shown in Fig. 14.

As shown in Fig. 14(a), in Case 1, each DSO re-dispatches the DGs and FLs to raise the bus voltage at the beginning, so that the bus voltage will not drop below the permitted range after providing the power support. According to Fig. 14(b), in Case 2, the bus voltage after re-dispatching is reduced so that enough power support can be provided, while avoiding the bus voltage beyond its upper limit. In Case 1 and Case 2, the voltage at the TSO-DSO interface has risen by 0.003 p.u. and dropped by 0.002 p.u. respectively after the re-dispatching in the distribution systems. However, the values are much smaller and do not influence the operation of the T-D system.

TABLE IX
POWER SUPPORTS IN EACH CASES

Case No.	Power Support			ΔV_{97}
	Resource	P	Q	
1	bus 96	5 MW	105 Mvar	0.01 p.u.
	bus 96 + DSOs	bus 96: -0.05 MW DSOs: 5.1 MW	bus 96: 65 Mvar DSOs: 21 Mvar	0.01 p.u.
2	bus 96	-5 MW	-110 Mvar	-0.01 p.u.
	bus 96 + DSOs	bus 96: 0.2 MW DSOs: -5.2 MW	bus 96: -38 Mvar DSOs: -19.5 Mvar	-0.01 p.u.

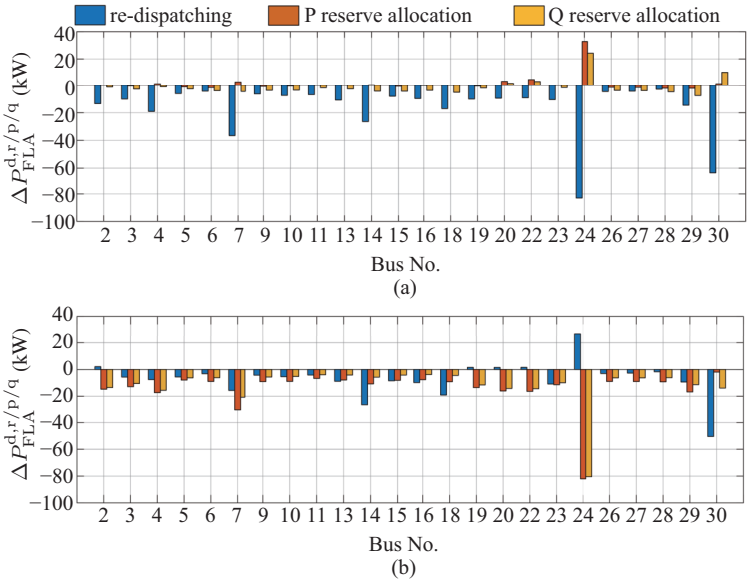

Fig. 13. The re-dispatching and reserve allocation results of FLs at each bus. (a) Case 1. (b) Case 2.

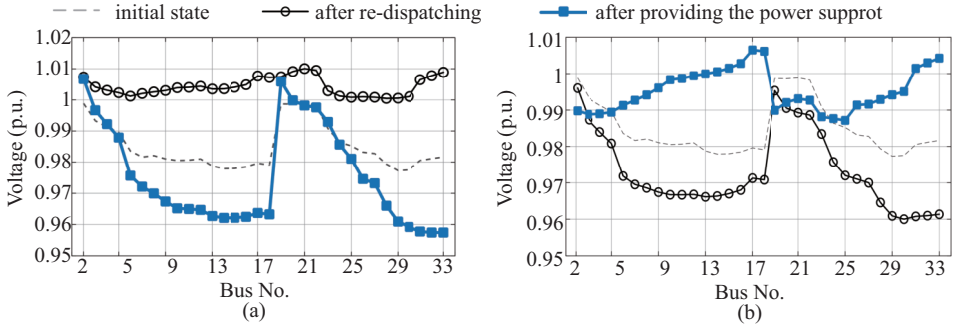

Fig. 14. The bus voltage results of each distribution system after two cases. (a) Case 1. (b) Case 2.

Therefore, it is verified that in the V-PQRC model-based T-D system coordination, the DSO can provide relatively accurate power support to the TSO while ensuring the inside voltage security. The TSO only needs to issue the reserve request according to the V-PQRC model, and the DSO can respond reliably, which is more efficient and convenient for the practical operation.

VII. Conclusion

To exploit the reserve potential of distribution systems in support of the transmission system operations, this paper proposes an evaluation method of the voltage-dependent P-Q reserve capacity (V-PQRC) at the TSO-DSO interface, considering uncertainties of DGs and FLs. Compared with the existing studies, the proposed method has the following features:

1) The proposed V-PQRC evaluation method captures the influence of the voltage deviation limit at the TSO-DSO interface on the feasible P-Q reserve capacity, for the sake of ensuring the distribution system voltage security. The simulation results reveal that extending the feasible P-Q reserve capacity region into a 3-D feasible space brings more information and higher accuracy, and also makes the T-D coordination operation more efficient.

2) The established GRCC-CSMC multi-objective optimization model for V-PQRC evaluation presents better performance in terms of accuracy and robustness compared with the single GRCC optimization, because the CSMC is able to drive FLs to respond as expected against their uncertainties, while providing the power support.

3) The proposed NAS method can significantly reduce the complexity of the V-PQRC model while maintaining a relatively high evaluation accuracy and robustness. The simulation results demonstrate that by using the V-PQRC model, the TSO can treat distribution systems as virtual voltage-dependent P-Q reserve resources while ensuring the operation security inside distribution systems. Therefore, it can significantly relieve the reserve capacity shortage of the transmission system, and reduce additional investment cost for increasing the transmission system reserve capacity.

Appendix

A. Proof of Theorem 1

To verify the reachability of the sliding surface, substitute (12) into the expression of $\dot{s}_{\mathrm{FLA},i}$, then (A1) is obtained.

$$T_{\mathrm{FL},i}\dot{s}_{\mathrm{FL},i} = \omega_{\mathrm{FL},i} - k_{\mathrm{FL},i}|s_{\mathrm{FL},i}|^{1/2}\operatorname{sgn}(s_{\mathrm{FL},i}) - s_{\mathrm{FL},i} \tag{A1}$$

A Lyapunov function $V_i = T_{\mathrm{FL},i}s_{\mathrm{FL},i}^2/2$ is constructed, and the time differential form $\dot{V}_i$ is formulated by (A2).

$$\begin{aligned}\dot{V}_{\mathrm{FL},i} &= T_{\mathrm{FL},i}s_{\mathrm{FL},i}\dot{s}_{\mathrm{FL},i}\\ &= -s_{\mathrm{FL},i}^2 + s_{\mathrm{FL},i}(\omega_{\mathrm{FL},i} - k_{\mathrm{FL},i}|s_{\mathrm{FL},i}|^{1/2}\operatorname{sgn}(s_{\mathrm{FL},i}))\\ &= -s_{\mathrm{FL},i}^2 + s_{\mathrm{FL},i}\omega_{\mathrm{FL},i} - k_{\mathrm{FL},i}|s_{\mathrm{FL},i}||s_{\mathrm{FL},i}|^{1/2}\end{aligned} \tag{A2}$$

Ensure that $\|\omega_{\mathrm{FL},i}\| \le \overline{\omega}_{\mathrm{FL},i}$, (A3) is valid:

$$\dot{V}_{\mathrm{FL},i} \le -s_{\mathrm{FL},i}^2 + |s_{\mathrm{FL},i}|(\bar{\omega}_{\mathrm{FL},i} - k_{\mathrm{FL},i}|s_{\mathrm{FL},i}|^{1/2}) \tag{A3}$$

Expand the constraint of $\Delta u_{\mathrm{FL},i}$ in (8). (A4)–(A5) are obtained:

$$\Delta P_{\mathrm{FL},i}^{\mathrm{down}} \le \Delta P_{\mathrm{FL},i}^{\mathrm{d}} - k_{\mathrm{FL},i}|s_{\mathrm{FL},i}|^{1/2}\operatorname{sgn}(s_{\mathrm{FL},i}) \le \Delta P_{\mathrm{FL},i}^{\mathrm{up}} \tag{A4}$$

$$\begin{cases} |s_{\mathrm{FL},i}|^{1/2} \le \dfrac{1}{k_{\mathrm{FL},i}}(\Delta P_{\mathrm{FL},i}^{\mathrm{up}} - \Delta P_{\mathrm{FL},i}^{\mathrm{d}}), & s_{\mathrm{FL},i} < 0\\ |s_{\mathrm{FL},i}|^{1/2} \le \dfrac{1}{k_{\mathrm{FL},i}}(\Delta P_{\mathrm{FL},i}^{\mathrm{d}} - \Delta P_{\mathrm{FL},i}^{\mathrm{down}}), & s_{\mathrm{FL},i} > 0 \end{cases} \tag{A5}$$

When $\Delta P_{\mathrm{FL},i}^{\mathrm{d}}$ is bounded by (13), (A6) can be deduced.

$$\begin{cases} \Delta P_{\mathrm{FL},i}^{\mathrm{up}} - \Delta P_{\mathrm{FL},i}^{\mathrm{d}} \ge \bar{\omega}_{\mathrm{FL},i}\\ \Delta P_{\mathrm{FL},i}^{\mathrm{d}} - \Delta P_{\mathrm{FL},i}^{\mathrm{down}} \ge \bar{\omega}_{\mathrm{FL},i} \end{cases} \tag{A6}$$

Consequently, we can draw the conclusion that:

$$\exists s_{\mathrm{FL},i} \in \text{(B3)},\ |s_{\mathrm{FL},i}| \ge \frac{\bar{\omega}_{\mathrm{FL},i}^2}{k_{\mathrm{FL},i}^2},\ \text{i.e.,}\ \dot{V}_i \le 0$$

By properly selecting $k_{\mathrm{FL},i}$ to make $\overline{\omega}_{\mathrm{FL},i}^2/k_{\mathrm{FL},i}^2 \to 0$, we can consider that $\dot{V}_i \le 0$ is always true, so that the sliding surface can be reached in finite time with the bounded $\Delta u_{\mathrm{FL},i}$.

B. Proof of the Duality Theory-based Reformulation Method

Use the first generalized robust chance constraint in (29) as an example, *abbr.* (29-1), to illustrate the derivation of the proposed reformulation method.

Let $b_i := V_i^{(0)} + \Delta V_i^{\mathrm{r}} + \boldsymbol{S}_{\mathrm{V-V},i}\Delta V_{\mathrm{PCC}}^*$, and $\xi_i := -\boldsymbol{S}_{\mathrm{V-P},i}^{\mathrm{DG}}(\boldsymbol{\omega}_{\mathrm{DG}} - \boldsymbol{\theta}_{\mathrm{DG}}) + b_i$. The left term of (29-1) is equivalent to the minimization problem (B1) based on [22] and Lemma 1 in [34].

$$\min \int h(\xi_i)g(\xi_i)\mathrm{d}\xi_i$$

s.t.

$$\begin{cases} h(\xi_i) = \begin{cases} 1 & \underline{V}_i + S_{\mathrm{V-P},i}^{\mathrm{DG}}\boldsymbol{\theta}_{\mathrm{DG}} \le \xi_i \le \overline{V}_i + S_{\mathrm{V-P},i}^{\mathrm{DG}}\boldsymbol{\theta}_{\mathrm{DG}}\\ 0 & \text{otherwise} \end{cases}\\ \int g(\xi_i)\mathrm{d}\xi_i = 1\\ -2\sqrt{\gamma_1}\sqrt{\hat{\Sigma}_{\mathrm{V},i}} + b_i \le \int \xi_i g(\xi_i)\mathrm{d}\xi \le 2\sqrt{\gamma_1}\sqrt{\hat{\Sigma}_{\mathrm{V},i}} + b_i\\ \int \xi_i^2 g(\xi_i)\mathrm{d}\xi_i \le b_i^2 + 2\sqrt{\gamma_1}\sqrt{\hat{\Sigma}_{\mathrm{V},i}} + \gamma_2\hat{\Sigma}_{\mathrm{V},i}\\ \int \xi_i^2 g(\xi_i)\mathrm{d}\xi_i \ge b_i^2 - 2\sqrt{\gamma_1}\sqrt{\hat{\Sigma}_{\mathrm{V},i}} + \gamma_2\hat{\Sigma}_{\mathrm{V},i} \end{cases} \tag{B1}$$

The dual problem of (B1) can be organized as (B2).

$$\max_{\lambda_i,\pi_i,\beta_i,\delta_i} \lambda_i + b_i\pi_i + (\gamma_2\hat{\Sigma}_{\mathrm{V},i} + b_i)^2\beta_i^2 - 2\sqrt{\gamma_1}\sqrt{\hat{\Sigma}_{\mathrm{V},i}}\delta_i$$

$$\text{s.t.} \quad \begin{cases} \lambda_i + \xi_i\pi_i + \xi_i^2\beta_i \le 1,\ h(\xi_i) = 1\\ \lambda_i + \xi_i\pi_i + \xi_i^2\beta_i \le 0,\ h(\xi_i) = 0\\ \beta_i < 0,\ \delta_i \ge 0 \end{cases} \tag{B2}$$

where λ_i, π_i, β_i, and δ_i are the dual multipliers.

To make the constraint (29-1) tractable, (B3) should be valid.

$$\exists \lambda_i + b_i\pi_i + (\gamma_2\hat{\Sigma}_{\mathrm{V},i} + b_i)^2\beta_i^2 - 2\sqrt{\gamma_1}\sqrt{\hat{\Sigma}_{\mathrm{V},i}}\delta_i \ge 1 - \mu_{\mathrm{V}} \tag{B3}$$

Similar as the proof of Theorem 2 in [22], (B1) and (B3) can be organized as (B4) by the Fourier-Motzkin elimination.

$$\begin{cases} y_i^2 + 2\sqrt{\gamma_1}\sqrt{\hat{\Sigma}_{\mathrm{V},i}}\pi_i\delta_i + (\gamma_2 - \gamma_1\delta_i^2)\hat{\Sigma}_{\mathrm{V},i} \\ \quad \le \mu_{\mathrm{V}}(\underline{V}_i + S^{\mathrm{DG}}_{\mathrm{V-P},i}\boldsymbol{\theta}_{\mathrm{DG}} - \pi_i)^2 \\ \underline{V}_i + S^{\mathrm{DG}}_{\mathrm{V-P},i}\boldsymbol{\theta}_{\mathrm{DG}} \le \pi_i \le \overline{V}_i + S^{\mathrm{DG}}_{\mathrm{V-P},i}\boldsymbol{\theta}_{\mathrm{DG}} \\ \delta_i \ge 0 \\ y_i = V_i^{(0)} + \Delta V_i^{\mathrm{r}} + S_{\mathrm{V-V},i}\Delta V^*_{\mathrm{PCC}} + \sqrt{\gamma_1}\sqrt{\hat{\Sigma}_{\mathrm{V},i}}\delta_i - \pi_i \end{cases} \tag{B4}$$

Since $\delta_i \ge 0$ and $\underline{V}_i + \boldsymbol{S}^{\mathrm{DG}}_{\mathrm{V-P},i}\boldsymbol{\theta}_{\mathrm{DG}}$ is always positive, the nonlinear constraints (B4) can be relaxed to (33).

C. Main Procedure of The NSGA-II Algorithm

The main procedure is listed as an Algorithm. According to (14)–(17), there are 8 combinations of the objectives, and each combination is optimized separately to improve the diversity of Pareto optimal solutions.

Algorithm 2: NSGA-II Algorithm for V-PQRC Evaluation

Input: number of iterations *Gen*; number of chromosomes *POP*
Output: Pareto optimal solution set S_{r}, which is initialized to $\varnothing$

initialize the chromosome population P_0 of size *POP*
$P_0 \leftarrow$ fast constrained-nondominated sorting (P_0)
Main Loop:
for $\eta_1, \eta_2, \eta_3 \in \{-1, 1\}$ **do**
  Select half of P_0 on behalf of the parent population P_1;
  for *iteration = 1 to Gen* **do**
    Create a new offspring population Q_2 of size *POP* from P_1 by selection, crossover and mutation operators;
    Obtain a combined population R_2: $R_2 = P_1 \cup Q_2$;
    Select the new parent population P_1 of size *POP* from R_2 by fast constrained-nondominated sorting and crowding distance operator;
  end
  Update S_{r}: $S_r = S_r \cup \{\text{chromosomes in Front}_1 \text{ of } P_1\}$
end
End

The parameters *POP* and *Gen* are set to 120 and 80 respectively. As a result, 960 Pareto optimal solutions can be obtained after the main loop, which can ensure diversity. Each Pareto optimal solution cannot be constrained-dominated by any other solution.

To improve the convergence performance, instead of the traditional random generation method, the chromosome population is initialized by repeatedly solving the single- objective optimization problem (C1) by randomly selecting the weights for each objective at each repetition.

$$\begin{aligned} \max F_i(\boldsymbol{x}_i) = {} & w_1\frac{F_1(\boldsymbol{x}_i) - F_1^{\min}}{F_1^{\max} - F_1^{\min}} + w_2\frac{F_2(\boldsymbol{x}_i) - F_2^{\min}}{F_2^{\max} - F_2^{\min}} \\ & + w_3\frac{F_3(\boldsymbol{x}_i) - F_3^{\min}}{F_3^{\max} - F_3^{\min}} \\ \text{s.t.} \quad & \begin{cases} \eta_1 = \eta_2 = \eta_3 = 1 \\ \boldsymbol{\Phi}: \begin{cases} \boldsymbol{A}_{\mathrm{eq}}\boldsymbol{x}_i + \boldsymbol{B}_{\mathrm{eq}} = 0 \\ \boldsymbol{A}_{\mathrm{ieq}}\boldsymbol{x}_i + \boldsymbol{B}_{\mathrm{ieq}} \le 0 \end{cases} \end{cases} \end{aligned} \tag{C1}$$

where $\boldsymbol{x}_i$ is the optimal solution and recognized as the i-th initial chromosome; $F_1^{\min}$ and $F_1^{\max}$, $F_2^{\min}$ and $F_2^{\max}$, $F_3^{\min}$ and $F_3^{\max}$ are the minimum and maximum values of F_1, F_2 and F_3 respectively; w_1, w_2 and w_3 are the weights, randomly selected from $[-1, 1]$.

Furthermore, the constrained-domination principle [35] is relaxed in this paper to ensure its solvability. The feasibility error is proposed to distinguish whether the constraints are satisfied, and is formulated by (C2).

$$E_i = (\boldsymbol{A}_{\mathrm{eq}}\boldsymbol{x}_i + \boldsymbol{B}_{\mathrm{eq}})^{\mathrm{T}}(\boldsymbol{A}_{\mathrm{eq}}\boldsymbol{x}_i + \boldsymbol{B}_{\mathrm{eq}}) + G(\boldsymbol{x}_i)^{\mathrm{T}}G(\boldsymbol{x}_i) \tag{C2}$$

where E_i is the feasibility error of solution i, representing the distance from the system security constraint set $\boldsymbol{\Phi}$; function $G(\boldsymbol{x}_i)$ satisfies $G(\boldsymbol{x}_i) = \max(\boldsymbol{A}_{i\mathrm{eq}}\boldsymbol{x}_i + \boldsymbol{B}_{i\mathrm{eq}}, 0)$.

The solution i is said to be a constrained-dominated solution j, if one of the following conditions is true:

1) The feasibility error of solution i is less than the threshold E_{th} while the solution j is not.

2) The feasibility errors of both solutions are beyond E_{th}, but solution i owns a smaller feasibility error.

3) The feasibility errors of solution i and j are both less than E_{th}. The three objectives of solution i are less than or equal to the objectives of solution j, and at least one objective of solution i is less than solution j.

D. Reserve Allocation for The Maximum Inductive Q Reserve

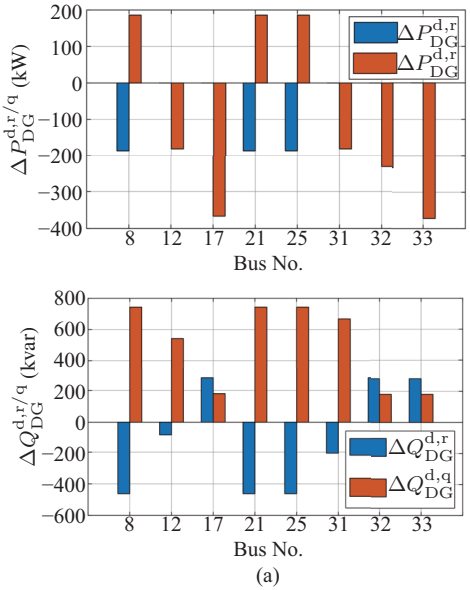

(a)

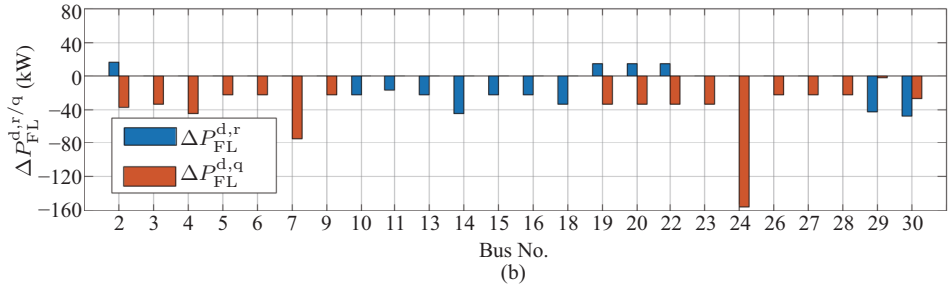

Fig. D1. The reserve allocation among DGs and FLs. (a) Reserve allocation results of DGs. (b) Reserve allocation results of FLs.

REFERENCES

[1] Q. H. Wu, A. Bose, C. Singh, J.H. Chow, G. Mu, Y. Sun, Z. Liu, Z. Li, and Y. Liu, "Control and Stability of Large-scale Power System with Highly Distributed Renewable Energy Generation: Viewpoints from Six Aspects," *CSEE Journal of Power and Energy Systems*, vol. 9, no. 1, pp. 8–14, Jan. 2023.

[2] H. B. Sun, Q. L. Guo, J. J. Qi, V. Ajjarapu, R. Bravo, J. Chow, Z. S. Li, R. Moghe, E. Nasr-Azadani, U. Tamrakar, G. N. Taranto, R. Tonkoski, G. Valverde, Q. W. Wu, and G. Y. Yang, "Review of challenges and research opportunities for voltage control in smart grids," *IEEE Transactions on Power Systems*, vol. 34, no. 4, pp. 2790–2801, Jul. 2019.

[3] A. La Bella, M. Farina, C. Sandroni, and R. Scattolini, "Design of aggregators for the day-ahead management of microgrids providing active and reactive power services," *IEEE Transactions on Control Systems Technology*, vol. 28, no. 6, pp. 2616–2624, Nov. 2020.

[4] Z. Chen, Z. S. Li, C. X. Guo, J. H. Wang, and Y. Ding, "Fully distributed robust reserve scheduling for coupled transmission and distribution systems," *IEEE Transactions on Power Systems*, vol. 36, no. 1, pp. 169–182, Jan. 2021.

[5] B. Hu, Y. Sun, C. Z. Shao, M. Shahidehpour, Y. Ding, T. Niu, and K. G. Xie, "A decentralized market framework for procurement of operating reserves from district energy systems," *IEEE Transactions on Sustainable Energy*, vol. 12, no. 3, pp. 1629–1639, Jul. 2021.

[6] J. Zhao, H. T. Wang, Y. T. Liu, Q. W. Wu, Z. Y. Wang, and Y. Liu, "Coordinated restoration of transmission and distribution system using decentralized scheme," *IEEE Transactions on Power Systems*, vol. 34, no. 5, pp. 3428–3442, Sep. 2019.

[7] C. Liu and P. W. Du, "Participation of load resources in day-ahead market to provide primary-frequency response reserve," *IEEE Transactions on Power Systems*, vol. 33, no. 5, pp. 5041–5051, Sep. 2018.

[8] S. Karagiannopoulos, C. Mylonas, P. Aristidou, and G. Hug, "Active distribution grids providing voltage support: The Swiss case," *IEEE Transactions on Smart Grid*, vol. 12, no. 1, pp. 268–278, Jan. 2021.

[9] F. Hinz and D. Möst, "Techno-economic evaluation of 110 kV grid reactive power support for the transmission grid," *IEEE Transactions on Power Systems*, vol. 33, no. 5, pp. 4809–4818, Sep. 2018.

[10] L. D. P. Ospina and T. Van Cutsem, "Emergency support of transmission voltages by active distribution networks: A non-intrusive scheme," *IEEE Transactions on Power Systems*, vol. 36, no. 5, pp. 3887–3896, Sep. 2021.

[11] S. Stanković and L. Soder, "Analytical estimation of reactive power capability of a radial distribution system," *IEEE Transactions on Power Systems*, vol. 33, no. 6, pp. 6131–6141, Nov. 2018.

[12] S. Stanković and L. Söder, "Probabilistic reactive power capability charts at DSO/TSO interface," *IEEE Transactions on Smart Grid*, vol. 11, no. 5, pp. 3860–3870, Sep. 2020.

[13] M. Heleno, R. Soares, J. Sumaili, R. J. Bessa, L. Seca, and M. A. Matos, "Estimation of the flexibility range in the transmission-distribution boundary," in *Proceedings of 2015 IEEE Eindhoven PowerTech*, Eindhoven, Netherland, 2015.

[14] J. Silva, J. Sumaili, R. J. Bessa, L. Seca, M. A. Matos, V. Miranda, M. Caujolle, B. Goncer, and M. Sebastian-Viana, "Estimating the active and reactive power flexibility area at the TSO-DSO interface," *IEEE Transactions on Power Systems*, vol. 33, no. 5, pp. 4741–4750, Sep. 2018.

[15] Z. F. Tan, H. W. Zhong, Q. Xia, C. Q. Kang, X. S. Wang, and H. H. Tang, "Estimating the robust P-Q capability of a technical virtual power plant under uncertainties," *IEEE Transactions on Power Systems*, vol. 35, no. 6, pp. 4285–4296, Nov. 2020.

[16] Z. S. Li, J. H. Wang, H. B. Sun, F. Qiu, and Q. L. Guo, "Robust estimation of reactive power for an active distribution system," *IEEE Transactions on Power Systems*, vol. 34, no. 5, pp. 3395–3407, Sep. 2019.

[17] Tyler Summers, Joseph Warrington, Manfred Morari, et al, "Stochastic optimal power flow based on conditional value at risk and distributional robustness," *International Journal of Electrical Power & Energy Systems*, vol.72, pp. 116–125, Nov. 2015.

[18] A. Zare, C. Y. Chung, J. P. Zhan, and S. O. Faried, "A distributionally robust chance-constrained MILP model for multistage distribution system planning with uncertain renewables and loads," *IEEE Transactions on Power Systems*, vol. 33, no. 5, pp. 5248–5262, Sep. 2018.

[19] Y. L. Zhang, S. Q. Shen, and J. L. Mathieu, "Distributionally robust chance-constrained optimal power flow with uncertain renewables and uncertain reserves provided by loads," *IEEE Transactions on Power Systems*, vol. 32, no. 2, pp. 1378–1388, Mar. 2017.

[20] A. P. Zhou, M. Yang, M. Q. Wang, and Y. M. Zhang, "A linear programming approximation of distributionally robust chance-constrained dispatch with Wasserstein distance," *IEEE Transactions on Power Systems*, vol. 35, no. 5, pp. 3366–3377, Sep. 2020.

[21] L. Dong, J. Li, T. J. Pu, and N. S. Chen, "Distributionally robust optimization model of active distribution network considering uncertainties of source and load," *Journal of Modern Power Systems and Clean Energy*, vol. 7, no. 6, pp. 1585–1595, Oct. 2019.

[22] E. Delage and Y. Y. Ye, "Distributionally robust optimization under moment uncertainty with application to data-driven problems," *Operations Research*, vol. 58, no. 3, pp. 595–612, Jan. 2010.

[23] A. P. Zhou, M. Yang, Z. Y. Wang, and P. Li, "A linear solution method of generalized robust chance constrained real-time dispatch," *IEEE Transactions on Power Systems*, vol. 33, no. 6, pp. 7313–7316, Nov. 2018.

[24] H. Khaloie, F. Vallée, C. S. Lai, J. F. Toubeau, and N. D. Hatziargyriou, "Day-ahead and intraday dispatch of an integrated biomass-concentrated solar system: A multi-objective risk-controlling approach," *IEEE Transactions on Power Systems*, vol. 37, no. 1, pp. 701–714, Jan. 2022.

[25] W. Du, W. M. Zhong, Y. Tang, W. L. Du, and Y. C. Jin, "High-dimensional robust multi-objective optimization for order scheduling: A decision variable classification approach," *IEEE Transactions on Industrial Informatics*, vol. 15, no. 1, pp. 293–304, Jan. 2019.

[26] Y. Y. Xu, L. Z. Yao, S. Y. Liao, Y. P. Li, J. Xu, and F. Cheng, "Optimal frequency regulation based on characterizing the air conditioning cluster by online deep learning," *CSEE Journal of Power and Energy Systems*, vol. 8, no. 5, pp. 1373–1387, Sep. 2022.

[27] A. Bilh, K. Naik, and R. El-Shatshat, "Evaluating electric vehicles' response time to regulation signals in smart grids," *IEEE Transactions on Industrial Informatics*, vol. 14, no. 3, pp. 1210–1219, Mar. 2018.

[28] J. Y. Hung, W. Gao, and J. C. Hung, "Variable structure control: A survey," *IEEE Transactions on Industrial Electronics*, vol. 40, no. 1, pp. 2–22, Feb. 1993.

[29] Y. Mi, Y. Fu, C. S. Wang, and P. Wang, "Decentralized sliding mode load frequency control for multi-area power systems," *IEEE Transactions on Power Systems*, vol. 28, no. 4, pp. 4301–4309, Nov. 2013.

[30] Y. Mi, Y. Ma, X. He, X. Yang, J. Gong, Y. Zhao, R. Liu, and W. Wei, "Robust Load Frequency Control for Isolated Microgrids Based

on Double-loop Compensation," *CSEE Journal of Power and Energy Systems*, vol. 9, no. 4, pp. 1359–1369, Jul. 2023.
[31] Q. X. Shi, F. X. Li, Q. R. Hu, and Z. W. Wang, "Dynamic demand control for system frequency regulation: Concept review, algorithm comparison, and future vision," *Electric Power Systems Research*, vol. 154, pp. 75–87, Jan. 2018.
[32] Y. Zheng, C. C. Zhang, D. J. Hill, and K. Meng, "Consensus control of electric spring using back-to-back converter for voltage regulation with ultra-high renewable penetration," *Journal of Modern Power Systems and Clean Energy*, vol. 5, no. 6, pp. 897–907, Nov. 2017.
[33] A. Bärmann, A. Heidt, A. Martin, S. Pokutta, and C. Thurner, "Polyhedral approximation of ellipsoidal uncertainty sets via extended formulations: A computational case study," *Computational Management Science*, vol. 13, no. 2, pp. 151–193, Apr. 2016.
[34] M. R. Wagner, "Stochastic 0–1 linear programming under limited distributional information," *Operations Research Letters*, vol. 36, no. 2, pp. 150–156, Mar. 2008.
[35] F. Pourahmadi, J. Kazempour, C. Ordoudis, P. Pinson, and S. H. Hosseini, "Distributionally robust chance-constrained generation expansion planning," *IEEE Transactions on Power Systems*, vol. 35, no. 4, pp. 2888–2903, Jul. 2020.
[36] W. J. Xie and S. Ahmed, "Distributionally robust chance constrained optimal power flow with renewables: A conic reformulation," *IEEE Transactions on Power Systems*, vol. 33, no. 2, pp. 1860–1867, Mar. 2018.
[37] K. Deb, A. Pratap, S. Agarwal, and T. Meyarivan, "A fast and elitist multiobjective genetic algorithm: NSGA-II," *IEEE Transactions on Evolutionary Computation*, vol. 6, no. 2, pp. 182–197, Apr. 2002.
[38] M. E. Baran and E. F. Wu, "Network reconfiguration in distribution systems for loss reduction and load balancing," *IEEE Transactions on Power Delivery*, vol. 4, no. 2, pp. 1401–1407, Apr. 1989.
[39] Elia Group. Wind power generation. [Online]. Available: https://www.elia.be/en/grid-data/generation-data/wind-power-generation. [2024-05-27].

Yeyan Xu received B.S. and M.S. degrees in Electrical Engineering from Wuhan University, Wuhan, China, in 2016 and 2019, respectively. She is currently pursuing a Ph.D degree in Electrical Engineering at the School of Electrical Engineering and Automation, Wuhan University. Her research interests include demand response, control strategies of demand response resources for power system operations, and power system economic operations.

Liangzhong Yao received M.S and Ph.D. degrees in Electrical Engineering from Tsinghua University, Beijing, China, in 1989 and 1993, respectively. He was a postdoctoral research associate at the University of Manchester from 1995 to 1999, was a Senior Power System Analyst at ABB in the UK from 1999 to 2004, and was Department Manager and Senior Expert at Alstom Grid Research and Technology Center in the UK from 2004 to 2011. From 2011 to 2018, he served as Vice President, respectively, at the State Grid Electric Power Research and China Electric Power Research Institute. He is now the Director of the Smart Grid Research Institute, and a Professor in the School of Electrical Engineering and Automation,Wuhan University. His current research interests include the integration technology of large-scale renewable energy, operation and control of AC-DC and DC grids. He has published over 350 journal and conference papers, over 60 patents, and 5 books or book chapters.

Tianjiao Pu received B.E. and M.Sc. degrees from Tianjin University, Tianjin, China, in 1992 and 1997, respectively. Since 1997, he is a Professor Senior Engineer with the China Electric Power Research Institute (CEPRI), a Fellow of IET, senior member of IEEE, senior member of the Chinese Society for Electrical Engineering, CIGRE member, Secretary General of the AI Committee of CSEE, deputy editor-in-chief of the IET Smart Grid. His research interests include power dispatching automation, smart grid simulation, active distribution network, and artificial intelligence.

Siyang Liao received B.S. and Ph.D. degrees in Electrical Engineering from Wuhan University, Wuhan, China, in 2011 and 2016, respectively. He is currently a Postdoctor in the School of Electrical Engineering, Wuhan University. His research interests include wind power integration and power system simulation technology.

Fan Cheng received a B.S. degree in Electrical Engineering and Automation from South China University of Technology, Guangzhou, China in 2014 and an M.Eng. degree in Electrical Engineering from Southeast University, Nanjing, China, in 2010. He has achieved a Ph.Eng. degree in Electrical Engineering at China Electric Power Research Institute in 2021, Beijing, China. Currently, he is a research asistant at Wuhan University. His research interests include large-scale renewable energy integration and interaction stability analysis of electronics.

Ye Li received an M.S. degree at North China Electric Power University in 2015, Beijing, China, and has worked in the Artificial Intelligence Application Research Section of China Electric Power Research Institute (CEPRI), Beijing, China, until now. She is the secretary of the IEEE PES Sub-committee on Power System Communications and Artificial Intelligence. Her research interests include distributed energy optimization scheduling and electric power artificial intelligence.

Xinying Wang received a Ph.D. degree from Dalian University of Technology, Dalian, China, in 2015, and has worked at China Electric Power Research Institute (CEPRI), Beijing, China, until now. He is the Deputy Director of Artificial Intelligence Application Research Section of CEPRI, the member of CSEE. His research interest includes electric artificial intelligence.